INVESTIGATION OF EYE FUNDUS IMAGE QUALITY ON VASCULAR SEGMENTATION USING DEEP NEURAL NETWORKS

Master Thesis

Systems biology master program

Vilnius university

STUDENT NAME: Julija Domarkaitė

STUDENT NUMBER: 2011285

SUPERVISOR: dr. Jolita Bernatavičienė

SUPERVISOR DECISION: **……**

FINAL GRADE **……**

DATE OF SUBMISSION: 13 05 2022

CONTENTS

LIST OF ABBREVIATIONS

Age-related macular degeneration (AMD)

Area under the curve (AUC)

Armed Forces Institute of Ophthalmology (AFIO)

Bi-Directional ConvLSTM (BConvLSTM)

Bi-Directional ConvLSTM U-net (BCDU-Net)

Contrast limited adaptive histogram equalization (CLAHE)

Convolutional neural network (CNN)

Deep Neural Network (DNN)

Diabetic macular oedema (DME)

Diabetic retinopathy (DR)

Digital retinal images for vessel extraction (DRIVE)

False positive (FP)

False negative (FN)

Field of view (FOV)

High -Resolution Fundus (HRF)

Hypertensive retinopathy (HR)

Non-proliferative diabetic retinopathy (NPDR)

Optic disk (OD)

Parametric ReLU (PReLU)

Proliferative diabetic retinopathy (PDR)

Rectified linear unit (ReLU)

Rectified Local Phase Unit (ReLPU)

Region of interest (ROI)

Residual U-net (ResUnet)

Spatial Attention U-net (SA-Unet)

Systemic hypertension (SH)

True positive (TP)

True negative (TN)

INTRODUCTION

The analysis of retinal fundus images with non-invasive medical imaging lets diagnose or track the progression of the diseases like diabetic retinopathy (DR), diabetic macular oedema (DME), age related macular degeneration (AMD), glaucoma, systemic hypertension (SH) and hypertensive retinopathy (HR). Morphological changes in retinal blood vessels are observed in DR, SH, and HR which if not detected early can lead to vision loss or even life-threatening complications (Kabedi et al., 2014; Wong and Sabanayagam, 2020). The analysis of the overall health of vasculature tree and vessel structural changes in fundus images is a reliable tool for the early detection of mentioned diseases.

The uniqueness of vasculature structures and enormous amounts of fundus images complicate manual segmentation making it ineffective in the modern world due to the huge time consumption needed for fundus image analysis (Chalakkal and Abdulla, 2017; Sosale, 2019). The improved deep learning methodology for segmentation have shown promising results in creating reliable assistance tool for ophthalmologists to make faster diagnoses. Even though, created model has to be universally applicable – be able to perform well on images of different quality and properties by providing reliable and robust segmentation results. This is where the problems arise as a lot of algorithms are built and optimised on one dataset with specific image quality and properties (Abdulsahib et al., 2022) making it unable to perform well on diverse data (Shen et al., 2020). Model inability to handle heterogeneous data eliminates the possibility to adapt it to real-life scenarios.

This field still lacks investigation on the influence of image quality and its properties on the performance of the model. This investigation would provide greater insights on the best approaches in conducting retinal vessel segmentation on diverse and different data. Because of that, this master thesis is analysing the impact of image quality and size on the performance of Deep Neural Networks (DNNs) by analysing different approaches for handling heterogeneous data.

AIM AND TASKS

The master thesis aims to investigate the feasibility of retinal vascular segmentation using deep neural networks (DNNs) and to evaluate the impact of different image qualities on segmentation accuracy.

Tasks:

1. Identify the advantages and disadvantages of selected algorithms according to their performance on eye fundus images of different quality.
2. Evaluate the impact of image size on the segmentation results.
3. Evaluate the influence of different interpolations on heterogeneous data and its segmentation results.
4. Evaluate the input size effect on the segmentation results.

LITERATURE REVIEW

1.1. Diseases associated with retinal vascular changes

The retina is a layered tissue lining the entire back wall inside of the eye (except the area of the optic disc (OD)). It consists of different types of cells which have a specific function in sensing and converting the light into a neural signal – the form which can be processed in the brain. As the retina is one of the most metabolically active tissue, its integrity of structure and function highly depends on a regular oxygen supply (Kaur et al., 2008). Because of that, retinal tissue has a unique vascular system – dual circulation – which ensures to maintain efficient oxygenation (Mahabadi and Al Khalili, 2021).

The retina is the only part of the human body, in which blood circulation can be observed with non-invasive medical imaging by photographing the back of the eye (Ramos-Soto et al., 2021). By analysing retinal fundus images, diseases like diabetic retinopathy (DR), diabetic macular oedema (DME), age-related macular degeneration (AMD), glaucoma, and hypertension can be quickly diagnosed. The most severe lesions are caused by DR, glaucoma, and AMD as they eventually lead to blindness if not detected and treated early.

Morphological changes in retinal blood vessels are observed in DR and cardiovascular diseases like systemic hypertension (SH) and hypertensive retinopathy (HR). To this day DR, which is a complication of diabetes mellitus, is a leading cause of visual loss in adults. Hyperglycaemia (high glucose level in blood) plays a key role in damaging retinal vascularity and is associated with dilation of blood vessels and changes in blood flow, apoptosis of pericytes and endothelial cells which results in microaneurysms formation, impairment of blood-retinal barrier, capillary occlusion and retinal hypoxia (Wang and Lo, 2018). There are two phases of DR: non-proliferative diabetic retinopathy (NPDR) and proliferative diabetic retinopathy (PDR). Clinically NPDR indicates the early stage of the disease and shows alterations such as vascular permeability and capillary occlusion which cause lesions like microaneurysms (the earliest sign of DR) and haemorrhages (Pappuru et al., 2019; Wang and Lo, 2018). These two do not affect the vision and usually are asymptomatic but they indicate the progression of the disease. It is extremely important to spot these pathologies because they can be treated by laser surgery and the vision will stay unaffected. If the disease is left untreated it may advance into PDR when retinal tissue begins to lack oxygen (retinal hypoxia) and new abnormal blood vessels originate (neovascularization) causing vitreous haemorrhages or retinal detachment resulting in sudden vision loss (Kusuhara et al., 2018).

High blood pressure (SH) is the main factor causing vessels transformation and can complicates into HR. In principle, hypertension can lead to abnormalities which are also inherent in DR patients: lesions (microaneurysms, haemorrhages, exudates), changes in retinal blood vessels diameters (arteriolar narrowing) and architecture (tortuosity and branching) (Dai et al., 2020; Ikram et al., 2006). Hypertensive retinopathy rarely itself causes visual loss but is a huge risk factor for the development

of DR, glaucoma and AMD (Modi and Arsiwalla, 2022; Wong et al., 2007). Furthermore, it can lead up to life-threatening complications like congestive heart failure or stroke (Kabedi et al., 2014). Retinal image segmentation can prevent mentioned complications of diseases as the early changes of blood vessels are observed in fundus images.

1.2. Biomarkers segmented in fundus images

Regular monitoring of retinal vessel changes is performed in DR patients but there are no recommendations for routine screening for HR asymptomatic patients who have SH diagnosis (Tsukikawa and Stacey, 2020). DR screening programs include retinal fundus imaging and manual assessment of DR.

Fundus images are obtained by photographing the back of the eye. Fundus imaging (Figure 1) is defined as the process where 3D retinal semi-transparent tissues are represented in 2D images and are obtained by using the reflection of light (Abràmoff et al., 2010). In the past, DR screening was performed by stationary mydriatic fundus camera which required pupil dilation and was not practical in some countries due to the lack of ophthalmologists and eye clinics (Piyasena et al., 2019). Because of the disadvantages of mydriatic photography, non-mydriatic fundus imaging became a popular screening tool at a primary care level due to its portability and no need for a pupil dilation.

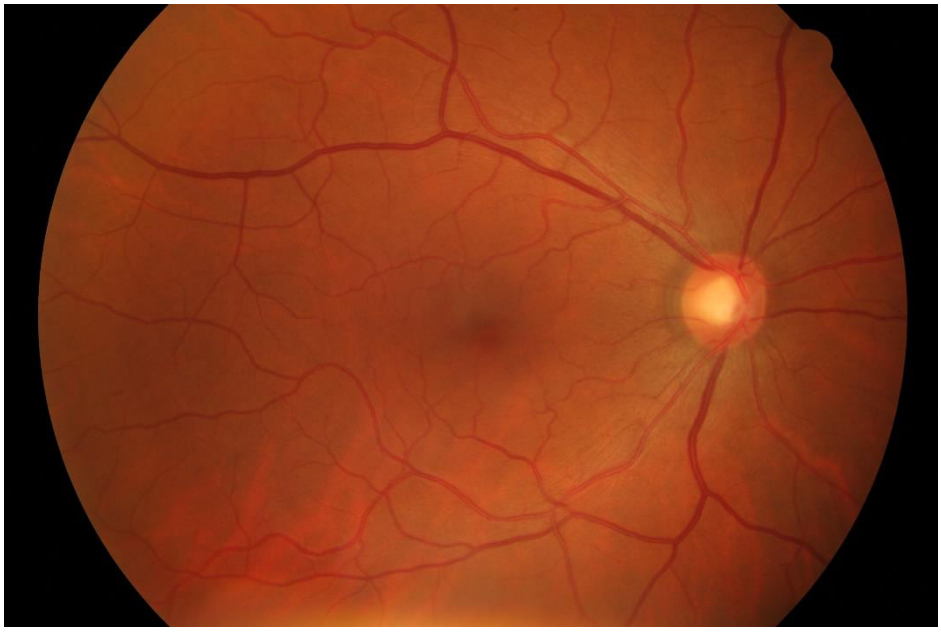

Figure 1. Normal retinal fundus image taken from HRF dataset (Budai et al., 2013)

From fundus images, structures of the eye (Figure 2), along with their location and shape, can be segmented. Alterations of biomarkers are associated with mentioned diseases: changes in OD with glaucoma; of macula and fovea – with DME or AMD; morphological changes of blood vessels are associated with DR, SH and HR. Different lesions can be represented in all diseases depending on

the stage of their progression. The analysis of vessel structural changes in fundus images is a reliable tool for the early detection of DR, SH and HR along with their progression. This analysis assesses the overall condition of the vascular tree and evaluates vessel morphological characteristics such as alterations of vessel tortuosity, narrowing, diameter/width, density and arteriolar-venular ratio (AVR) (Abdulsahib et al., 2021; Miri et al., 2017). In DR high glucose levels in the blood damage walls of thin vessels and vessels start leaking blood, forming microaneurysms near them. Furthermore, hyperglycaemia decreases the elasticity of vessels, causing them to narrow and their tortuosity transforms (Rosen et al., 2019). Fundus images from SH and HR patients can also display alterations in vascular narrowing and AVR (Oluleye et al., 2016).

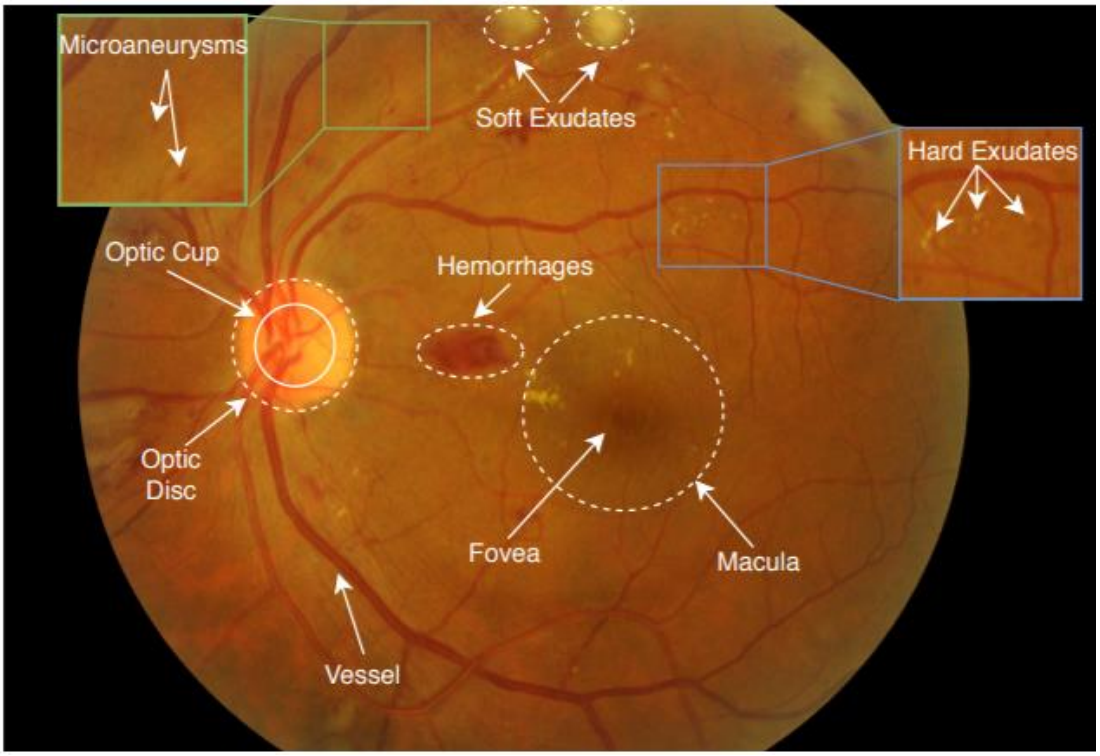

Figure 2. An eye fundus image with labelled biomarkers (Li et al., 2021)

From retinal fundus imaging it is possible to evaluate retinal vascularity manually or automatically. The main limitations of blood vessels manual segmentation are that it is time-consuming and could be led by errors even from experienced observers. It takes around one to two hours to manually segment a single fundus image while with automatic segmentation complete it takes less than a minute (Chalakkal and Abdulla, 2017). In addition, the number of people affected by retinal diseases is increasing globally and the field itself lacks qualified doctors to conduct analysis of retinal images (L Srinidhi et al., 2017; Sosale, 2019). This leads to growing fundus photography volumes causing delays in getting back results to patients. Furthermore, the extraction of retinal vasculature itself is a difficult task. It is because retinal vasculature is unique to every individual and stands out in the diversity of vessels shapes, sizes, widths, intensity and arrangements (crossing and branching) (Li

et al., 2018; Oliveira et al., 2018; Semerád and Drahanský, 2020). Besides the challenges which occur during discrimination of vessels, the low quality of images and occurred lesions in the retina cause segmentation to be even more complicated. Because of all mentioned reasons, the automatic, fast and most importantly accurate segmentation which could be an assisting tool for ophthalmologists to make a quick diagnosis of retinal changes is necessary (Boudegga et al., 2021).

1.3. Quality and size of fundus images

Image quality is a huge issue on any task based on computer vision, but especially for the retina as various factors affect the condition of the image. It is not easy to define what is a low or high quality image as it is more intuitive for a person individually decide. Even so, some quality criteria for fundus images could be singled out: image noise, illumination disparities, camera artefacts, presence of lesions caused by disease and contrast between the object and the background (Adapa et al., 2020; Pednekar et al., 2018). The images of the retina most often are affected by non-uniform illumination. It is caused by several factors: narrow lens in completely dilated pupil, variation in light reflection and diffusion, low contrast, noise, and differences in retinal pigmentation and cameras (Joshi, 2017). The deviation from any mentioned criteria highly complicates both manual and automatic segmentation of retinal vessels.

Nevertheless, the influence of image quality on automatic retinal vessel segmentation is yet little known as researches focus more on the development of a quality grading system for fundus images (Karlsson et al., 2021) and deep learning approaches: for classification of low quality regions in retinal images (Costa et al., 2017); classification of image quality regarding sharpness and illumination (Chalakkal et al., 2019) or differentiation of fundus images from optical coherence tomography images and classification of good quality images (Zapata et al., 2020). In real-life applications, for automatic segmentation of retinal vessels, not only effects of image quality need to be taken into consideration, but the impact of image size also. As automatic models are restricted to some size of the input, larger or smaller images need to be pre-processed by resizing. The modifications of size changes feature representation in the image (Rukundo, 2021) and it affects not only the segmentation performance but computational and memory requirements also which changes practical application effectiveness (Sahlsten et al., 2019). To conclude, it is necessary to assess mentioned details of the images in order to have robust and effectual segmentation of retinal blood vessels.

1.4. Automatic image segmentation

1.4.1. Neural networks

The main goal of image segmentation is to locate objects of interest (or their boundaries) by providing a simplified but more meaningful representation of the image for its easier analysis. Convolutional neural network (CNN) is the standard neural network architecture used for image analysis. In these networks, a mathematical operation – convolution – is employed. It produces a sum-of-product between input values and kernel weights while convoluting the smaller kernel over a larger image (Ghosh et al., 2019). Supervised methods became a popular approach in medical image segmentation. These methods rely on prior known information – the classifier is trained on manually labelled classes and segmented ground truth references, thereby creating rules for vessel pixel classification (Adapa et al., 2020).

For retinal blood vessel segmentation supervised model firstly extracts relevant features which patterns are learned automatically and after that pixels are classified (Chen et al., 2021). Because of efficiency of deep learning methods (mostly performance time and huge accuracy), lots of research is conducted in this field hoping to develop a robust model for application in real-life scenarios.

1.4.2. Related work

In 2015 Ronneberger et al. (2015) proposed the new convolutional neural network (CNN) architecture, called U-net. This architecture is very beneficial in the biomedical field because it can effectively work with fewer training images and provides more precise segmentation. The U-net differs from traditional CNN because it has not only a contracting (encoding) path but an expansive (decoding) path also (Figure 3). The contracting path is the same as in traditional CNN architecture consisting of four downsampling layers which are made of two 3x3 convolutions. Each convolution is followed by an activation function – rectified linear unit (ReLU). Every downsampling layer is followed by max pooling operation. After each downsampling step the size of the image reduces, but because of max pooling – which reduces the size of the feature map by selecting the maximum pixel value – the receptive field increases. Bridge connects encoding and decoding paths. In the expansive path, there are four upsampling layers, with also two convolutions. At every upsampling layer, the corresponding output from the encoding path is concatenated. These upsampling operators increase the resolution of the output. The higher resolution feature maps from the contracting path with the up-sample features ensure more precise prediction. Furthermore, in the decoding path, there is a large number of feature channels. Because of it, the network is able to propagate context information further, to higher resolution layers.

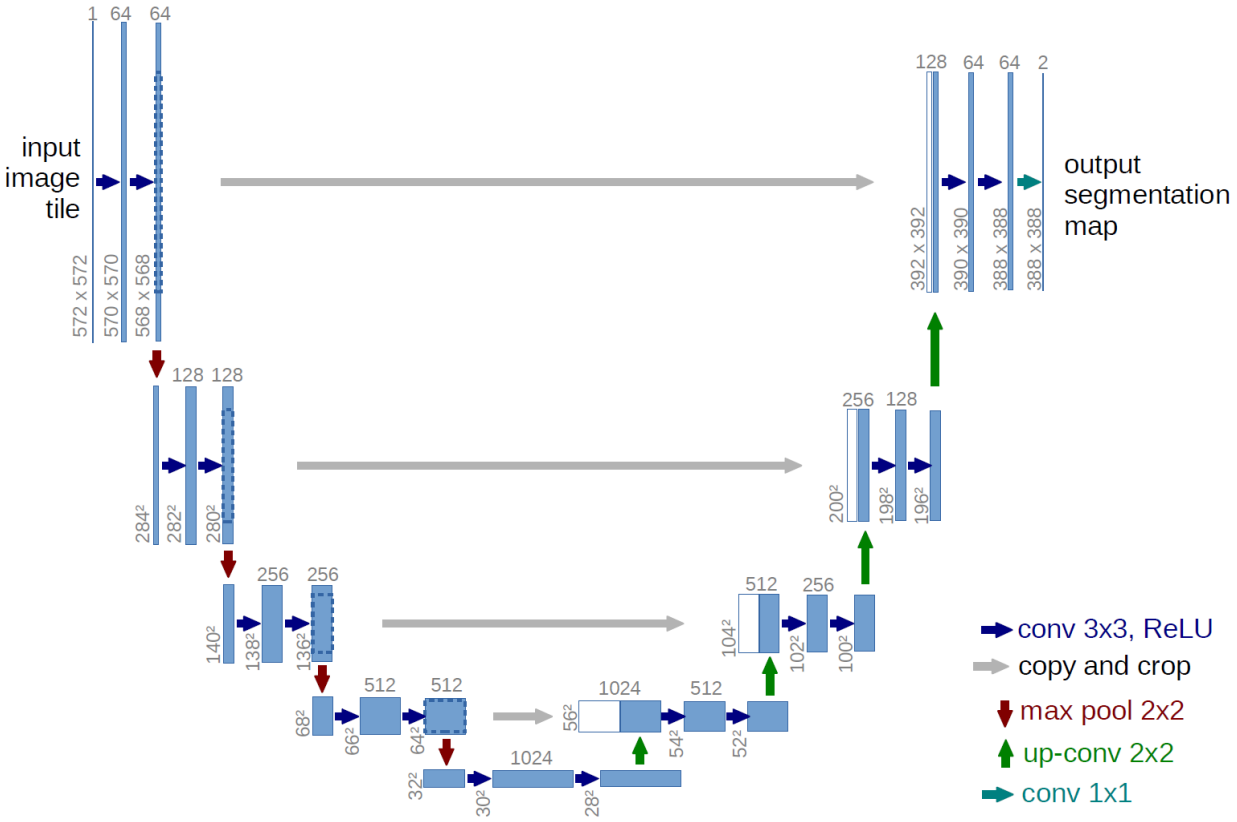

Figure 3. The architecture of U-net (Ronneberger et al., 2015)

Since the introduction of U-net, many scholars used this algorithm for retinal blood segmentation and proposed some architecture modifications in order to achieve better results in biomedical image segmentation. Xiuqin, et al. (Xiuqin et al., 2019) modified the traditional U-net by applying the Residual unit to the module in the expansive path. In the suggested method, the residual unit is implemented by the skip connection and the input is directly passed to the output. This improvement increases the training speed of the algorithm. Also, it solves the vanishing and exploding gradient problems which happen to very deep neural networks. Because the model ensures non-degrading information, the deeper network can be designed.

To solve the segmentation of thin vessels problem, the accuracy and sensitivity of the algorithm have to be improved. Gao, et al., (2017) proposed to combine U-net and Gaussian matched filter in order to resolve mentioned topic. The scholars choose a short period of the major blood vessel and many small blood vessels where their length is divided by 2 and the direction is fixed. The segmented small vessels are more robust and the upsampling layer of the expansive path does not recover details of coding loss effectively. Because of that, the sensitivity of the model is kind of low. Another method to resolve the segmentation of thin vessels problem was proposed by Cheng, et al. (2020) by adding the dense block to U-net. The dense block directly connects all layers – the input of each layer comes from the output of all previous layers. The network of Dense U-net is narrower with fewer parameters and this leads to better network performance. Also, parametric ReLU (PReLU) is used as the activation function. It avoids the death of neurons and has a fast convergence speed with no

vanishing gradient problem. The method achieved good sensitivity performance on CHASE_DB1 dataset, but the sensitivity on DRIVE database was poor.

To achieve better results of segmentation, Kumawat and Raman (2019) propose to insert Rectified Local Phase Unit (ReLPU) layer on the top of U-Net, after the input layer. The ReLPU layer itself is constructed of 4 layers: standard convolution, a second layer, which extracts local phase from the output of the first layer by computing the short term Fourier transforms in 2D space (image encoding) – network learns about frequency points and neighbourhood sizes – gives more weight to chosen ones in the fourth layer. The third layer is the ReLU activation layer and the fourth one is a trainable layer. ReLPU layer needs fewer learnable parameters than a convolutional layer, but further analysis of this layer application possibilities needs to be done. Another way to improve the algorithm was proposed by Kushol and Salekin (2020) by inserting the encoder ResNet152 inside the U-net architecture. ResNet152 contains 152 layers and this encoder optionally loads weights pre-trained. It achieved good sensitivity results on the STARE dataset. Soomro et al. (2018) proposed a fully-strided convolutional neural network (Strided U-net) for labelling every pixel in the image and classifying it as a background or a vessel pixel. In this algorithm, all pooling layers were replaced by strided convolutional layers. These layers not only do the same function as pooling layers but also decrease the size of the feature maps to half. The dice loss was chosen as the loss function as it has good accuracy segmenting thin vessels. The performance of the algorithm is not outstanding and the AUC value, which shows classification performance, is low. Sathananthavathi et al. (2021) proposed many changes to traditional U-net architecture. In order to increase the receptive field, all convolutional layers were replaced by dilated convolutional layers and in order not to exclude any features, all stages were assigned with an equal number of kernels. Dilated convolutions widen the kernel by inserting gaps between kernel elements. Receptive field increases without losing any resolution. Furthermore, in the encoding path, two additional layers were added resulting in a total number of 96 layers in the proposed architecture. Even though the proposed method achieved good specificity for the HRF dataset, the method not achieved great sensitivity for any analysed database. Hemelings et al. (2019) modify U-net by setting 3-channel RGB input at the encoding path and the output at the end of expanding path to four classes (background, vein, artery and unknown). These output maps are generated by the final convolutional layer which has four filters. To increase the receptive field, scholars increased the kernel of each convolution to 5x5 as dilation did not favour the DRIVE dataset. This improvement lets applicate the U-net (which was designed for image segmentation) for the classification of vessels. This method achieved high accuracy on the HRF dataset. Atli and Gedik (2021) introduced a pure novelty, fully convolutional model called Sine-Net. The proposed architecture first applies upsampling operations, which help to extract thin vessel features, and then downsampling operations for the extraction of thick vessel features. Furthermore, scholars used strided and transposed convolutions instead max-pooling and upsampling layers. Because of that, the method learns and updates weights during both downsampling and upsampling operations. Sine-Net achieved great specificity performance on all used datasets and all evaluation

metrics (despise sensitivity on STARE database) show great performance of the algorithm. The pathologies in STARE images probably affect the sensitivity of the segmentation but in the future, it can be resolved by choosing an appropriate loss function.

Guo et al. (2020) introduce Spatial Attention U-net (SA-Unet). This method replaces original convolutional blocks with structured dropout convolutional blocks which implement DropBlock (where neighbouring units of a feature map are dropped together) and batch normalization. These blocks prevent the overfitting of the algorithm. In the bridge, scholars apply the Spatial Attention Module which enhances important features and suppresses unimportant features by multiplying the attention map by the input feature map. Attention map is produced from the spatial relationship between features. SA-Unet achieves state-of-art performance on both DRIVE and CHASE_DB1 datasets by accuracy and AUC values close to 1. The performance of algorithms and used datasets for retinal blood vessel segmentation are shown in Table 1.

Table 1. The comparison of the proposed methods performance on different datasets for retinal blood vessel segmentation

Author	Method	Datasets	Performance			
			Accuracy	Sensitivity	Specificity	AUC
(Xiuqin et al., 2019)	Res U-net	DRIVE	0.965	**0.831**	0.9863	0.9811
(Gao et al., 2017)	U-net and Gaussian matched filter	DRIVE	0.9636	0.7802	**0.9876**	0.9772
(Hemelings et al., 2019)	FCN	DRIVE	0.9675	-	-	-
		HRF	**0.9698**	-	-	-
(Kumawat and Raman, 2019)	Local Phase U-net	DRIVE	-	-	-	0.9831
		STARE	-	-	-	0.9930
(Cheng et al., 2020)	Densely connected U-net	DRIVE	0.9559	0.7672	0.9834	0.9793
		CHASE_DB1	0.9488	**0.8967**	0.954	0.9785
(Kushol and Salekin, 2020)	RBVS-Net	DRIVE	0.9633	0.8003	0.9792	-
		CHASE_DB1	0.9675	0.7823	0.9801	-
		STARE	0.9708	**0.8188**	0.9824	-
(Soomro et al., 2018)	Strided U-net	DRIVE	0.948	0.739	0.956	0.844
		STARE	0.947	0.748	0.962	0.855
(Sathananthavathi et al., 2021)	EEA U-net	DRIVE	0.9577	0.7918	0.9708	-
		STARE	0.9445	0.8021	0.9561	-
		CHASE_DB1	0.9340	0.6457	0.9653	-
		HRF	0.9244	0.6589	**0.9799**	-
(Atli and Gedik, 2021)	Sine-Net (FCNN)	DRIVE	0.9685	0.8260	0.9824	0.9852
		STARE	**0.9711**	0.6776	**0.9946**	**0.9807**
		CHASE_DB1	0.9676	0.7856	**0.9845**	0.9828
(Guo *et al.*, 2020)	SA-UNet	DRIVE	**0.9698**	0.8212	0.984	**0.9864**
		CHASE_DB1	**0.9755**	0.8573	0.9835	**0.9905**

Literature analysis has shown that a huge variety of algorithms was proposed in order to resolve different retinal vessel segmentation tasks. Nevertheless, this field still lacks investigation on how

the properties of the image, especially image quality (Abdulsahib et al., 2022; Wan et al., 2022), influence the performance of the model. In addition, a lot of proposed methods are not yet suitable for real-life scenarios as algorithms are usually built and optimised just on one or few datasets with similar data characteristics (Abdulsahib et al., 2022; Memari et al., 2019) while population-level screening for retinal diseases always implies a huge variety of fundus cameras and the main target population presents vast variation in the health condition of retina (Shen et al., 2020). Greater insights into ability of models to conduct accurate segmentation of retinal vessels from images of different properties are necessary. This master thesis investigates, how image quality such as various types of illuminations, low resolution and size affects the performance of DNNs, as well as investigating the most suitable approaches (image size, resizing technique and input size) for the retinal vessel segmentation when dealing with heterogeneous data.

METHODS

2.1. Data

In the project 7 datasets, which are used in developing an automatic segmentation of retinal vessels for disease diagnosis and are available online, were collected and used for training and testing the algorithms. As supervised machine learning algorithms are used in the project, datasets containing at least one manual blood vessel annotation were chosen. The summary of collected data is presented in Table 2.

Table 2. Properties of collected data

Dataset	Camera	Number of images	Image size (width x height)
DRIVE	Canon CR5 3CCD	40	565x584
STARE	TRV-50	20	700x605
CHASE_DB1	–	28	999x960
IOSTAR	EasyScan	30	1024x1024
DRHAGIS	Canon CR Dgi, Topcon TRC-NW8, TRC-NW6s	39	4752x3168, 3216x2136, 3456x2304, 2816x1880, 2896x1944
ARVDB	Topcon TRC-NW8	100	1504x1000
HRF	–	45	3504x2336

The DRIVE (digital retinal images for vessel extraction) dataset was obtained from a diabetic retinopathy screening program performed in the Netherlands. The photographs were taken using a Canon CR5 non-mydriatic 3CCD camera whose field of view (FOV) is of 45 degrees. The dataset consists of 40 retinal images, where 33 images were observed from healthy patients and 7 images show early lesions of DR. The size of the images is 768x584 and the resolution of the images is 565x584. The dataset is divided into 20 training images and 20 testing images.

The STARE (structured analysis of the retina) database (Hoover *et al*, 2000) was conceived in 1975 at the university of California, San Diego by Michael Goldbaum, M.D. The dataset contains 20 images, and 10 of them show pathologies. All images are manually annotated by two observers, the first set is considered as the ground truth. Images were taken by a TRV-50 fundus camera with 35 FOV and have a resolution of 700x605 pixels.

The HRF (High-Resolution Fundus) database (Budai et al., 2013) consists of 45 fundus images which are divided into healthy, glaucoma and DR patients (15 images of each type). The resolution of the images is 3504x2336.

The CHASE_DB1 (Owen et al., 2009) dataset contains 28 fundus images, collected from both eyes of 14 children from London, Birmingham and Leicester. The resolution of the images is 999x960. All images are manually labelled by two experts.

The IOSTAR vessel segmentation dataset (Abbasi-Sureshjani et al., 2015; Zhang et al., 2016) includes 30 images which were taken using an EasyScan camera with FOV of 45 degree. The resolution of images is 1024x1024 pixels. Database was obtained from the RetinaCheck project which conducted a large-scale screening program of diabetes patients in China. The ground truths of vessel segmentation, artery/vein and OD are annotated by a group of experts.

The DRHAGIS database (Holm et al., 2017) consists of 39 fundus images obtained during DR screening program performed in the United Kingdom. Images were taken with 3 different non-mydriatic cameras (Canon CR DGi, Topcon TRC-NW8 and Topcon TRC-NW6s) with 45 FOV. As different cameras were used the resolution of images is not the same. Resolution varies from 4752x3168, 3216x2136, 3456x2304 to 2816x1880 or 2896x1944. Even though the resolution of images is the highest, some images have a large amount of lesions or uneven and low illumination which could cause bad segmentation of retinal vessels. On the contrary, in some of the high quality images the choroidal vessels are visible which could also contort the results. Choroid is a connective tissue layer with a dense network of vessels lying below the retina, which supplies nutrition to the outer retina and maintains the temperature of the eye (Ehrlich et al., 2017; Lambert-Cheatham et al., 2021). Choroidal vessels in fundus images are captured by multispectral fundus cameras with wavelengths longer than 605 nm (Huang et al., 2020). Mostly these vessels are brighter and thicker than retinal vessels, they do not come from the optic nerve and are not annotated in retinal vessels manual segmentation. Examples of images from DRHAGIS are presented in Figure 4.

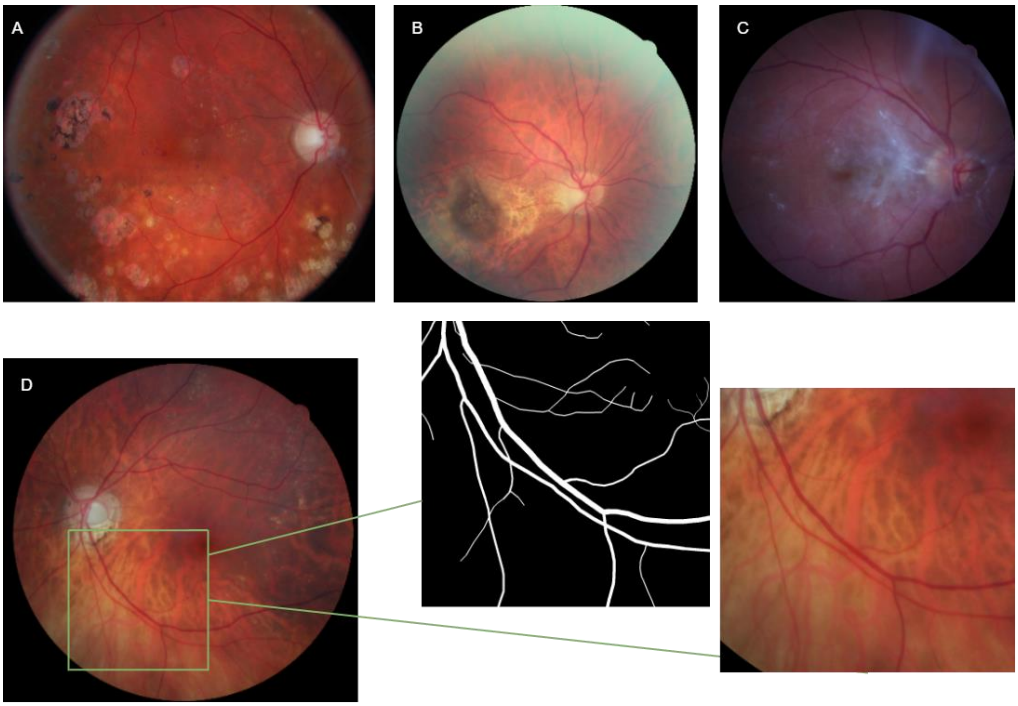

Figure 4. Images from DRHAGIS dataset. (A) – Image with lesions; (B) – Uneven illumination; (C) – Low illumination; (D) – High quality image with visible choroidal vessels

DRHAGIS dataset presents one manual segmentation annotated by an experienced observer. Images in this database were divided by visible lesions into four groups: glaucoma, hypertension, DR and AMD patients. One patient exhibited both DR and AMD co-morbidities and this image is included in both groups. Only one example of the image was used in our project to avoid any distortion of the results.

Another dataset (Akram et al., 2020) with an unspecified title (will be referred as ARVDB) contains 100 fundus images acquired from Armed Forces Institute of Ophthalmology (AFIO), Pakistan. Images were taken by a non-mydriatic TOPCON TRCN-W8 camera with 30 FOV. Resolution of the images is 1504x1000. Manual vessel segmentations were performed by four experts of AFIO. Two images were removed as corresponding manual segmentations were untrue to the original images. This dataset contains the highest amount of low quality images which examples are presented in Figure 5.

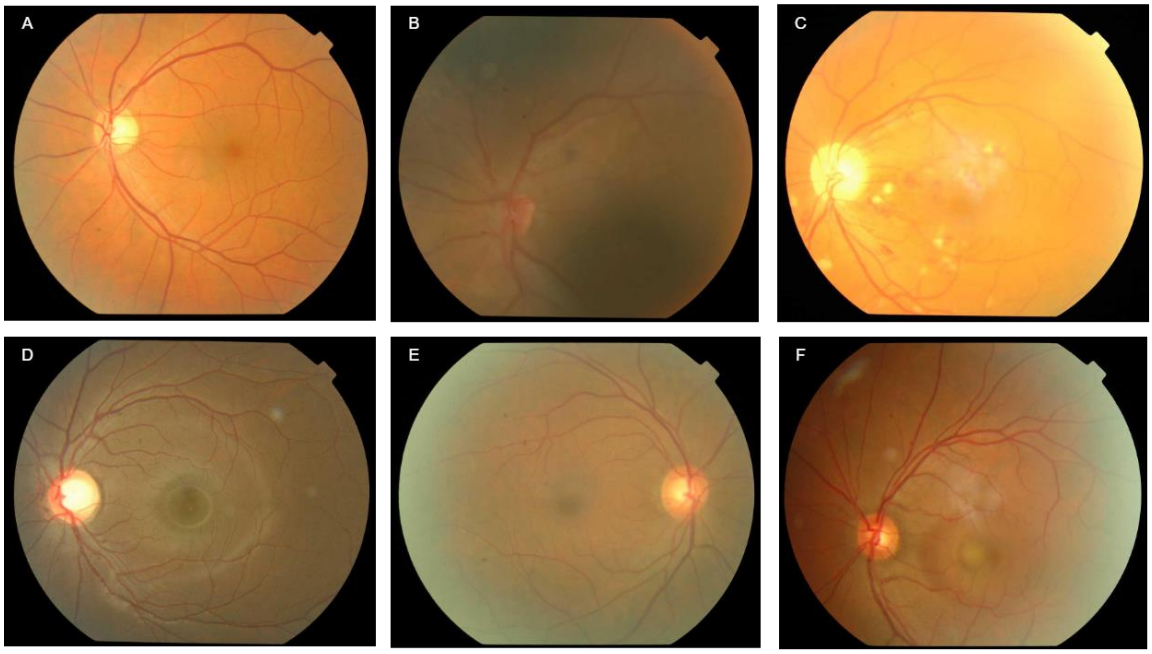

Figure 5. Images from ARVDB dataset. (A) – Good quality image; (B) – Parts of the image with low illumination; (C) – Blurred image; (D) – Camera artefact; (E) – Distortion of colour; (F) – Uneven illumination

Data in all datasets were divided into training and testing samples. As only the DRIVE dataset was separated by default to training and testing folders, we divided images from other datasets randomly: 80 percent of samples were assigned for training and the remaining samples to testing groups.

2.2. Data preparation, pre-processing and augmentation

To prepare suitable images for resizing, we removed the unnecessary background and left only the region of interest (ROI). Original images were converted to grayscale images which by thresholding were transformed to binary images. From binary images contours of the object (continuous points along the border of object) were found. Coordinates of contours were used for calculating minimal

bounding rectangles for non-zero pixels (object) and original images, ground truths and masks were cropped by their values. Extraction of the ROI guarantees an appropriate image interpolation without distorting characteristics of the object. The ground truths of ARVDB dataset were transformed to appropriate appearance as originally they represented vessels in black and background in white colours. It was done by changing values of pixels.

From datasets training and testing data (original images, corresponding ground truths and border masks) are saved in hdf5 format. This format supports large and heterogeneous data and is suitable for used algorithms. For samples of STARE, CHASE_DB1, ARVDB databases we automatically generated border masks as it was not provided primarily. Border masks are used to define the area of the FOV in fundus image so only area inside the FOV would be used for image segmentation and analysis. Border masks were obtained by thresholding original fundus images.

The pre-processing step is used to normalize the intensities of image by reducing/removing noise and enhancing contrast. It is essential point as limitation of undesired variance ensures that the dataset is consistent and displays only relevant features. Retinal images were pre-processed by converting original RGB images into grayscale images as true colours of fundus image complicates feature detection and segmentation (Hernandez-Matas et al., 2019). Pixels were divided by 255 to ensure that they fit into [0,1] range. In order to reduce noise and increase the contrast between vessels and background, contrast limited adaptive histogram equalization (CLAHE). When CLAHE is applied, image is divided into tiles of size 8x8 and histograms for each blocks are computed and interpolated values are assigned to neighbouring pixels of the centre pixel in tile. CLAHE improves local contrasts and definitions of edges in each region (Swathi et al., 2017). For further contrast enhancement, gamma correction were used. It suppresses the uneven light and corrects image in different regions by raising real pixel value to the power of gamma (Rahman et al., 2016).

As DNNs needs a lot of data to be trained, data is artificially augmented. In this project full size images are randomly split into smaller patches of size 64x64 and they can overlap by some amount of pixels. By giving patch as an input, DNNs acquire feature maps which at the end are concluded into the final segmented image.

2.3. The structure of deep neural networks

In this master thesis two DNNs – Bi-Directional ConvLSTM U-net (BCDU-Net) and Residual U-net (ResUnet) – will be used as they are based on U-net. BCDU-Net algorithm was proposed by Azad et al. (2019) and implements Bi-Directional ConvLSTM (BConvLSTM) and densely connected convolutions. The architecture of the network is presented in Figure 6.

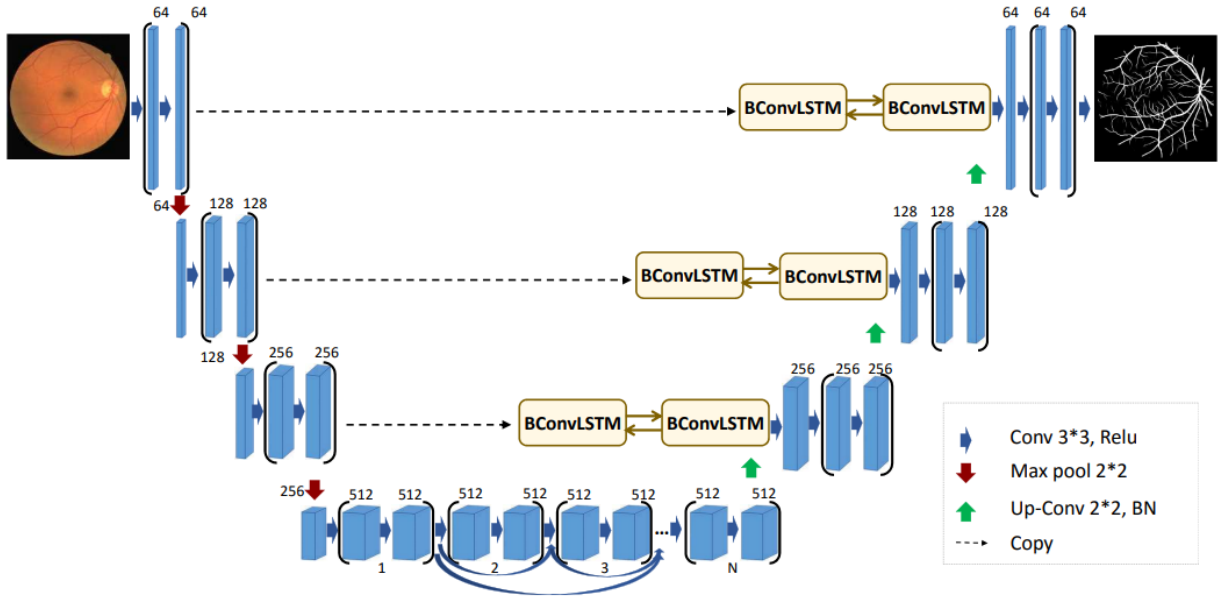

Figure 6. The structure of BCDU-Net algorithm (Azad et al., 2019)

The contracting path is identical to traditional U-net – there are three layers of two 3x3 convolutions followed by 2x2 max pooling operation and ReLU activation function: ReLU(x) = max{0, x}. ReLU is a piecewise linear function – it is linear if the input x has a positive value as it returns the value which was provided or nonlinear if the $x \leq 0$ as output will be 0 even when input had negative value.

The differences from U-net occurs in the bridge as it consists three layers of two 3x3 convolutions with ReLU function. Furthermore, the third bridge layer is densely connected to the first one which is concatenated with second convolutional block. Because of dense connectivity third convolutional block receives feature map not only from previous layer, but from first block also, meaning that algorithm learns diverse feature maps and the risk of vanishing or exploding gradients is avoided (Liu et al., 2021).

To the output of last layer of the bridge upsampling operation is employed, starting the expansive path. Upsampling operation seeks to restore original features and every upsampling operation as well as corresponding feature map from encoding path concatenated and fed to BConvLSTM layer. This layer uses two ConvLSTM layers which moves the input to forward and backward directions in their hidden tensors, dealing with data dependencies and makes a decision for the input. After that 2x2 convolutions are applied which at each step increases the size of the feature maps. It goes on until it reaches the final layer where sigmoid is used as activation function: Sigmoid(x) = $1/(1 + e^{-x})$ and produces values from 0 to 1 – standard output produced in segmentation.

Researchers introduced BCDU-Net as model which achieves high results in segmentation of various types of images: fundus; dermoscopy skin and lung computed tomography, which is really important for our case as we are focusing on analysing the best approach for segmentation of images with diverse features and properties. For retinal vessel segmentation task, BCDU-Net was trained and

tested only on DRIVE dataset, which have relatively little amount of images whose size is small. BCDU-Net performance shown in Table 3.

Table 3. The performance of BCDU-Net network on DRIVE dataset

Network	Accuracy	Sensitivity	Specificity	AUC	F1-score
BCDU-Net	0.9560	0.8007	0.9786	0.9789	0.8224

Originally ResUnet was proposed for semantic road extraction from aerial images by implementing residual units in U-net architecture (Zhang et al., 2018). As mentioned before, in 2019 Xiuqin et al. (2019), implemented ResUnet for vascular segmentation task. Same as BCDU-Net, ResUnet was also trained and tested only on DRIVE dataset and achieved accuracy, sensitivity, specificity and AUC of 0.9650, 0.8310, 0.9863 and 0.9811 respectively.This model replaces traditional neural units (two convolutions 3x3 with ReLU activation function) with residual units, where convolutions are followed by batch normalization and ReLU activation and most importantly have added shortcut/skip connections meaning that layer feeds into the next layer and directly into further layer. Both BCDU-Net and ResUnet use skip connections, but their implementation differs – in ResUnet shortcut connections are added and implemented throughout the structure, while in BCDU-Net they are only in the bridge and concatenated. When skip connections are summed, features are refined through the network layers and fixed amount of features is preserved across the unit. Meanwhile concatenated skip connections reuses middle representations – ensures the maximum information flow throughout layers and maintenance of enormous amount of features (Huang et al., 2018). Despite the advantages, concatenation can cause a rise of trainable parameters which would lead to drastically prolonged training time. The structure of ResUnet used in this master thesis is presented in Figure 7.

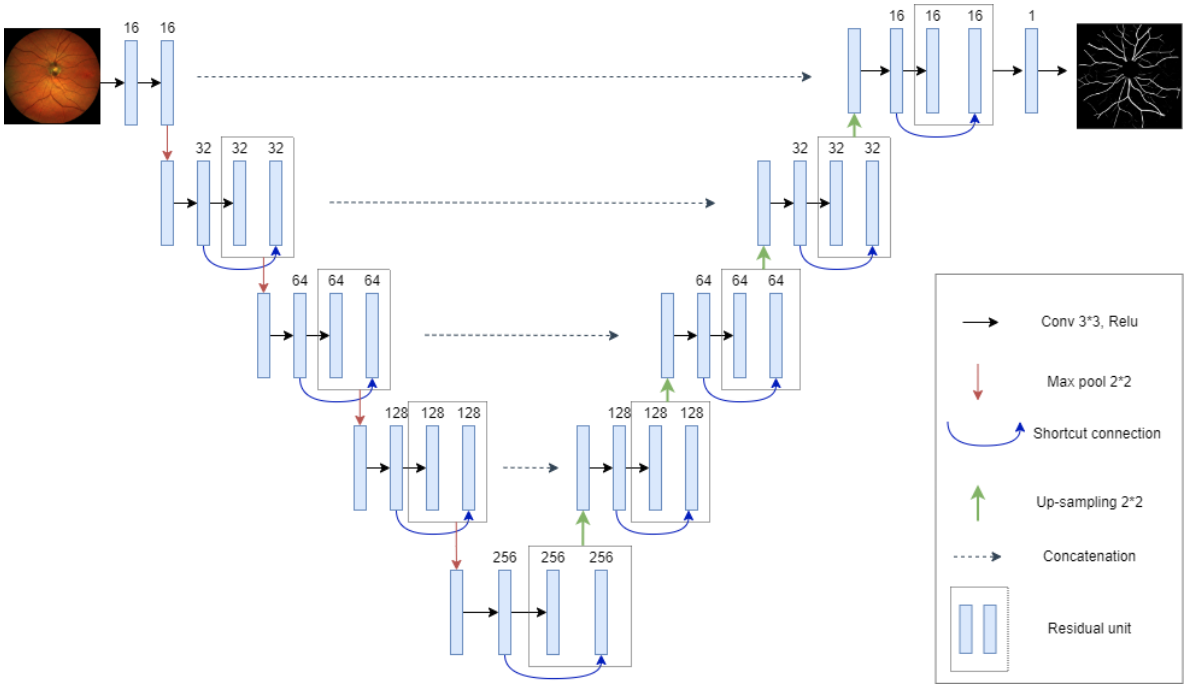

Figure 7. The architecture of ResUnet

Used ResUnet model has four downsampling and upsampling layers and one residual convolution layer at the bridge. At the end of encoding path the reached feature map of ResUnet is two times smaller than in BCDU-Net and overall there are three times less trainable parameters in ResUnet. This structure suggests that this algorithm requires less time to train. In addition, because of the shortcut connections throughout its structure, learning of the redundant features would be avoided which is important when dealing with diverse data.

To summarize, both algorithms were proposed on DRIVE dataset and achieved quite fine results in the task of retinal vessel segmentation. Even though, it is unclear how these models would perform on images of different properties and quality, which is exceptionally important in real-life situations. Because of that, our experiments compare these two models in two directions: their performance on different datasets when trained on DRIVE (as both models were proposed) and their performance when trained with heterogeneous data (training sets from all datasets combined into one), which is a usual case in real-life.

2.4. Image resizing by different interpolations

Till this day the effects of the image size from various databases for training the algorithms were vaguely analysed (Pauli et al., 2012; Rukundo, 2021). Even though as U-net based algorithms do not have fully connected layers and can process arbitrary sized inputs, the pixel aspect ratio highly differs when feeding large and small images into the networks. The algorithm trained on the vessels of the same size in pixels of some fixed resolution is going to fail on images with vessels of different size. Because of that, the segmentation performance of algorithms highly depends on the size of images used for vessel profile in the training stage. In order to investigate such size dependencies, our master thesis analyses the effects on network performance by resizing images with three nearest neighbour, bilinear and bicubic interpolations.

Image interpolation is a process which employs known data in estimating values at unspecified locations (Gonzalez and Woods, 2018). The geometrical transformations do not alter the content of the image but deform the grid of the pixel which is mapped to a goal image. The location of a pixel is denoted by 2-dimensional grid in an image $f(i, j)$, when referring to coordinates of a pixel (i, j). By interpolating the image, coordinates of the corresponding contributor pixel in original image is computed and intensity value is copied for each pixel (i, j) into the goal image:

$$\text{goal}(i, j) = \text{original}(f_x(i, j), f_y(i, j)) \quad (1)$$

From all interpolations the most straightforward one is a nearest neighbour interpolation. This interpolation does not create new pixel value but simply resamples the contributor pixel value to a neighbour empty location at the shortest distance. It is the computational fastest and simplest

approach but the main disadvantage appears by upscaling an image, when after the interpolation, pixels become much bigger and image along with its features appears to be blocky with degraded quality (Rukundo and Cao, 2012).

Bilinear interpolation takes values not from one nearest known neighbour as in nearest neighbour interpolation, but from four closest neighbouring pixels. The coordinates of these neighbouring pixels are (x_1, y_1), (x_1, y_2), (x_2, y_1) and (x_2, y_2) with values Z_{11}, Z_{12}, Z_{21}, Z_{22} at these points. By having values and coordinates of neighbouring pixels the value Z at (x, y) of goal pixel can be calculated by formula:

$$Z(x,y) = \frac{(x_2 - x)(y_2 - y)}{(x_2 - x_1)(y_2 - y_1)} Z_{11} + \frac{(x_2 - x)(y - y_1)}{(x_2 - x_1)(y_2 - y_1)} Z_{12} + \frac{(x - x_1)(y_2 - y)}{(x_2 - x_1)(y_2 - y_1)} Z_{21} + \frac{(x - x_1)(y - y_1)}{(x_2 - x_1)(y_2 - y_1)} Z_{22} \quad (2)$$

Where the weighted average of these pixel values is calculated and assigned at interpolated pixel. Bilinear interpolation takes more processing time to compute the final pixel than nearest neighbour interpolation and produces smoother images with blurred features (Bovik, 2009).

Bicubic interpolation fits a surface among four corner pixels by using a third order polynomial function (Khaledyan et al., 2020). The intensity values along with vertical, horizontal and vertical derivate of four corner points have to be specified in order to compute this interpolation. The interpolated surface $f_i(x, y)$ is presented as:

$$f_i(x,y) = \sum_{i=0}^{3} \sum_{j=0}^{3} a_{ij} x^i y^j \quad (3)$$

Where 16 coefficients of $a_{i,j}$ have to be determined (intensity values in four corners directly determines 4 coefficients, spatial derivate in the horizontal and vertical direction – 8 coefficients and diagonal derivatives – 4 coefficients) (Gao and Gruev, 2011). Basically, bicubic interpolation considers the closest known 4x4 neighbourhood pixels and closer pixels give higher weighting in the calculation than further ones. This method produces sharper images than previous interpolations and takes the longest processing time for computing a goal pixel.

For this master thesis, images was either reduced or increased in size as the data have different dimensions. The downsampling of image size is easier task than upsampling because by increasing the size, interpolation methods have to create artificial pixels to add into original image. However, when images are reduced in size the number of pixels are permanently removed and the quality of the image decreases. Furthermore, another problem arises – downscaling tends to deform the thinniest and smallest vessels as they are represented only by a few pixels. In resized ground truths these vessels lose connectivity and original form as some white pixels are removed. It becomes unclear from which branch vessel origins, where it ends and what shape it has. The ground truth is put into algorithms without the information of small vessels details and the performance results from algorithms can be affected. The examples of downscaled and upscaled retinal images and manual segmentations are presented in Figure 8.

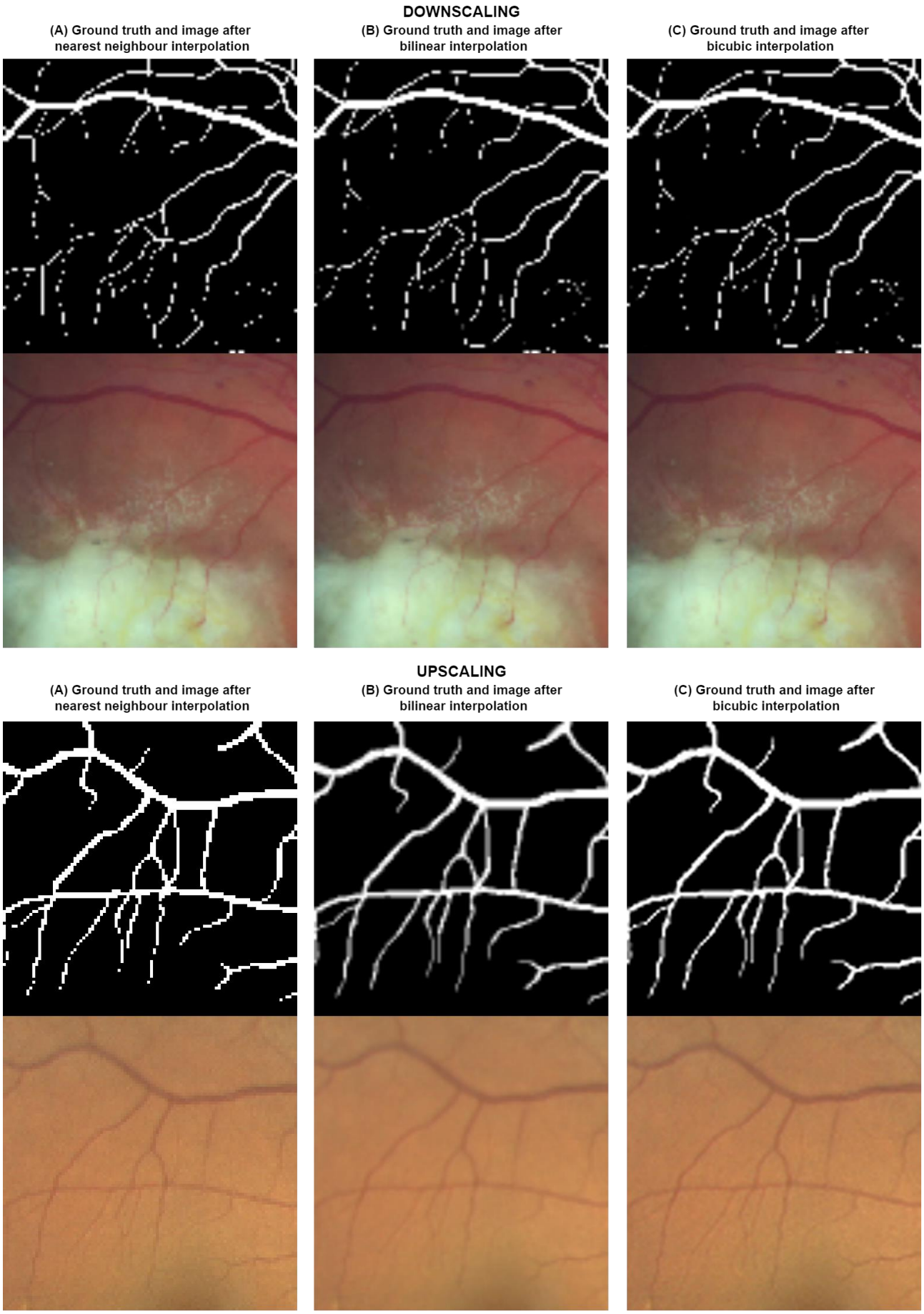

Figure 8. Resizing by different interpolations

By visually judging, it seems that nearest neighbour interpolation distort vessels and it representing pixels the most. In addition, bicubic and bilinear interpolations provide very similar outcomes just that bilinear interpolation smooths features more. Because of that bicubic interpolation gives an impression as the most appropriate resizing technique for accurate retinal vessel representation. In our experiments all three interpolations are evaluated with respect to their influence to the segmentation results.

2.5. The methodology of the master thesis

This master thesis is focusing on investigating the best approaches for retinal blood vessels segmentation with neural networks while working with datasets of different quality and size which at is an usual case in real word scenarios. The same data preparation, pre-processing and patch extraction techniques are used for all training and testing processes. In total 10 trainings for this master thesis were conducted. All trainings were carried out for 50 epochs with batch size of 32 and tested on all datasets separately, each time resizing (by the same interpolation used for training) the testing images to the size of the training images. All computations were done on VU MIF ITAPC supercomputer with 1912 CPU cores 17TB RAM and 32GPU 1TB RAM with 3xNVIDIA DGX-1 Tesla V100 system of 32GB graphic memory.

In the first experiment both DNNs are trained on DRIVE images from which 200000 patches (size 64x64) were extracted. Algorithms are trained only on DRIVE images as both models were proposed and evaluated only on this dataset. We evaluate both DNNs on other datasets also. All testing images are resized to the size of the 565x565 by nearest neighbour interpolation as it is the fastest technique and the first experiment is conducted in order to compare algorithms and select the model which performs better on diverse data without analysing the influence of interpolations to the performance of networks.

As we are focusing for the best segmentation on several datasets with different characteristics, both algorithms are trained on combined training set from all datasets (229 training images in total). We are hoping to simulate real-life situation when models have to perform well on diverse data. The training images of all datasets were resized by nearest neighbouring interpolation to the same dimensions (565x565) and 196940 patches were extracted. The combination of datasets was done in order to observe how much the performance of algorithms changes when patches contains more diverse features inside (tortuosity, size, branches, etc. of vessels, various lesions) and different quality of images (uneven illumination, blurriness, artifacts, etc.). The combination of training samples reduces redundancy as patches are extracted from 10 times larger amount of images. In addition, this step shows which model is able to accurately segmentate more diverse features and

is selected for further experiments The scheme of first experiment is present in Figure 9.

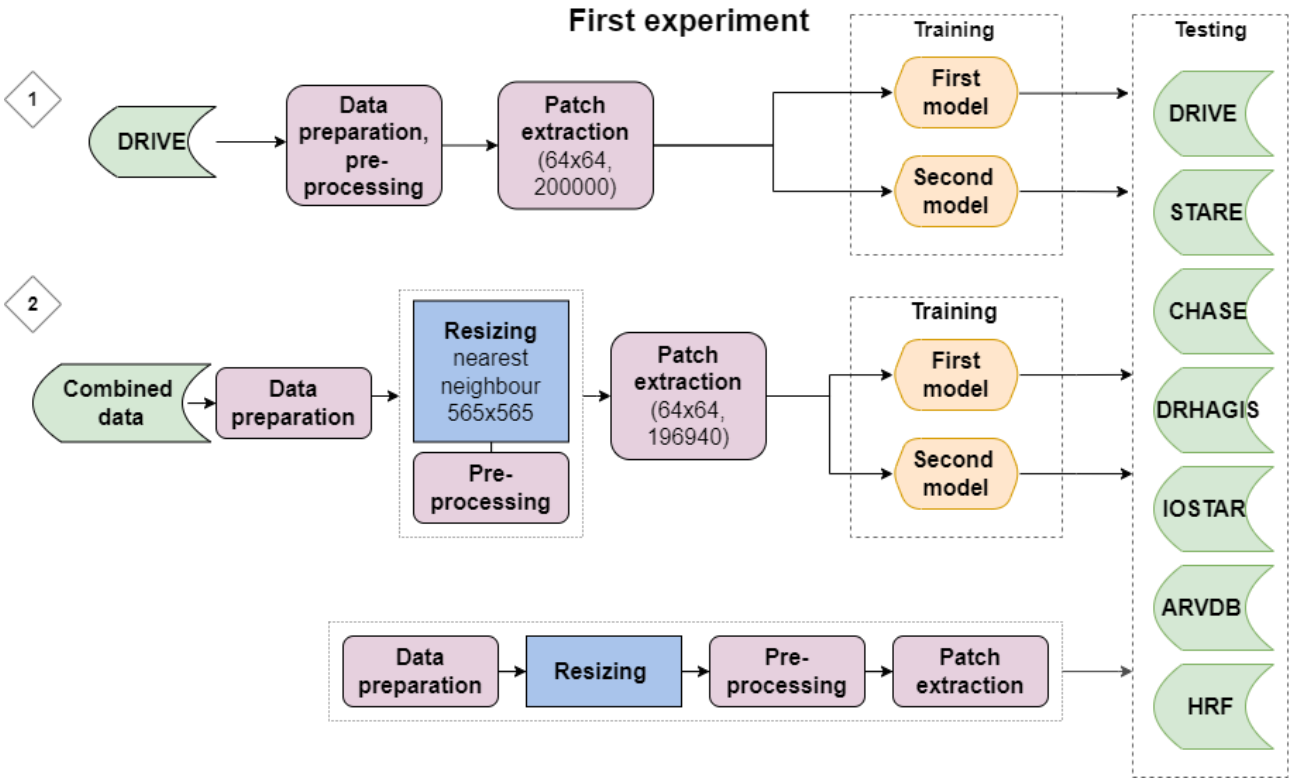

Figure 9. The scheme for model selection

Second experiment (Figure 10) is done in order to choose the most appropriate size of the images for the best segmentation of retinal blood vessels.

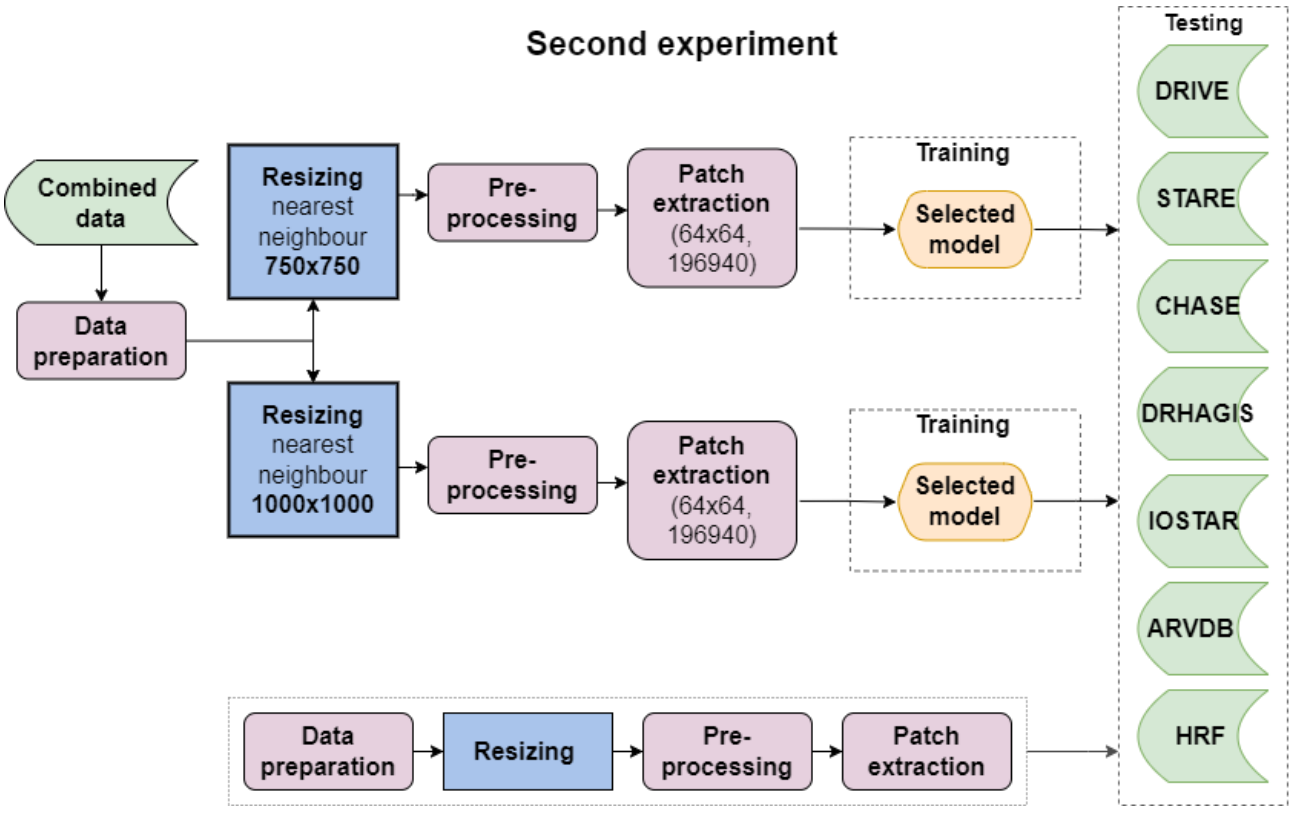

Figure 10. The scheme for image size selection

The combined data was resized to 750x750 and 1000x1000 using nearest neighbour interpolation. When images were resized to the size of DRIVE dataset, all images from other datasets lost some information because of downscaling (except DRIVE database). As mentioned before, downscaling disfigures and loses thin vessels – the ground truths are already put to model without truthful material which can produce unreliable results. By resizing to mentioned sizes the most convenient image size is selected which is favourable for diverse data, as it requires some images to be downscaled while loosing pixels and others to be upscaled with artificially created pixels.

In fourth experiment images are resized by bilinear and bicubic interpolations to the size selected in third experiment, in order to investigate the impact of different resizing techniques to the segmentation results. We explained differences between interpolations in 2.4. section and their effects on models performances were evaluated in this experiment. The interpolation giving the best results for segmentation is selected. The pipeline of experiment is presented in Figure 11.

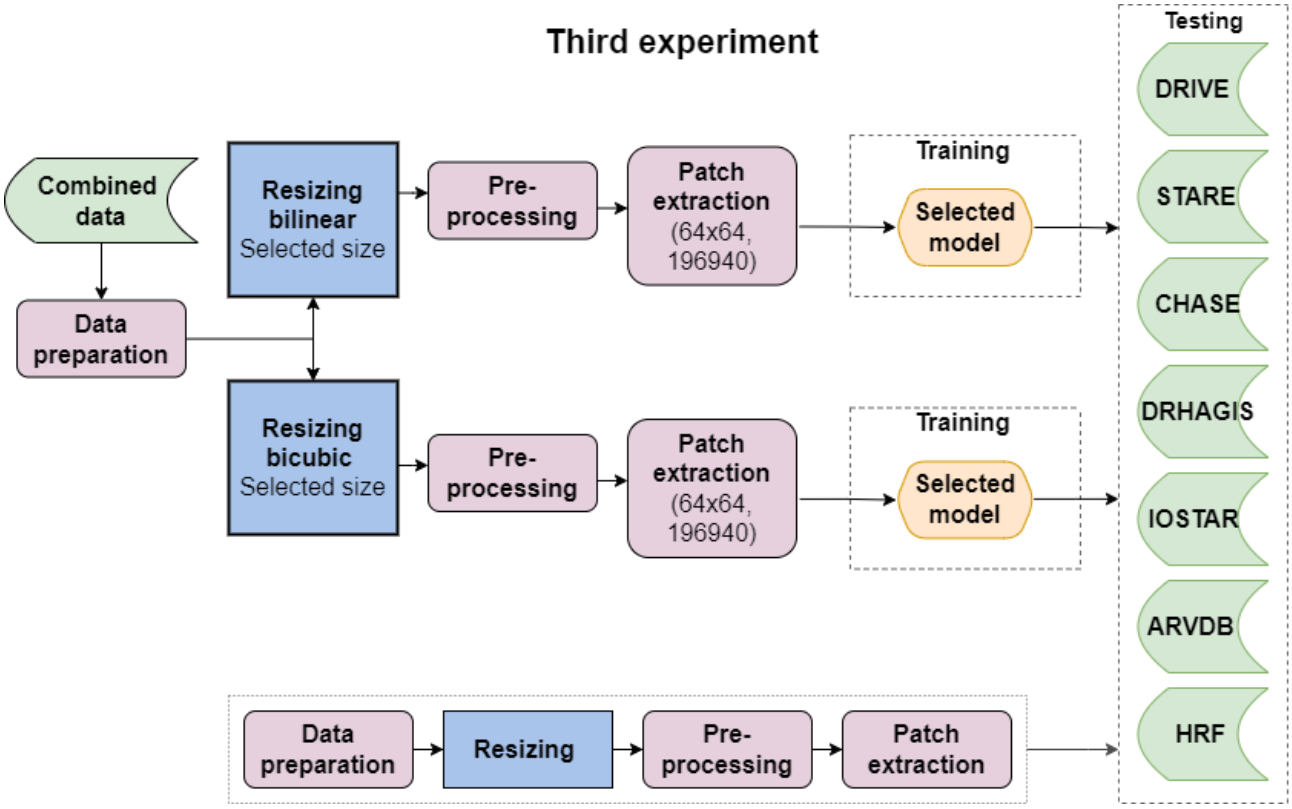

Figure 11. The scheme for interpolation selection

In the last experiment (Figure 12) the size of the input for the model is selected. As for all earlier experiments patches of size 64x64 was given to the model, this approach includes changing the input size to two times smaller (32x32) and two times larger (128x128). Inputs of different sizes parallelly provides different information from which model extracts feature maps and can make a decision when classifying pixels. The impact of input size on DNN training time and its performance effectiveness were evaluated.

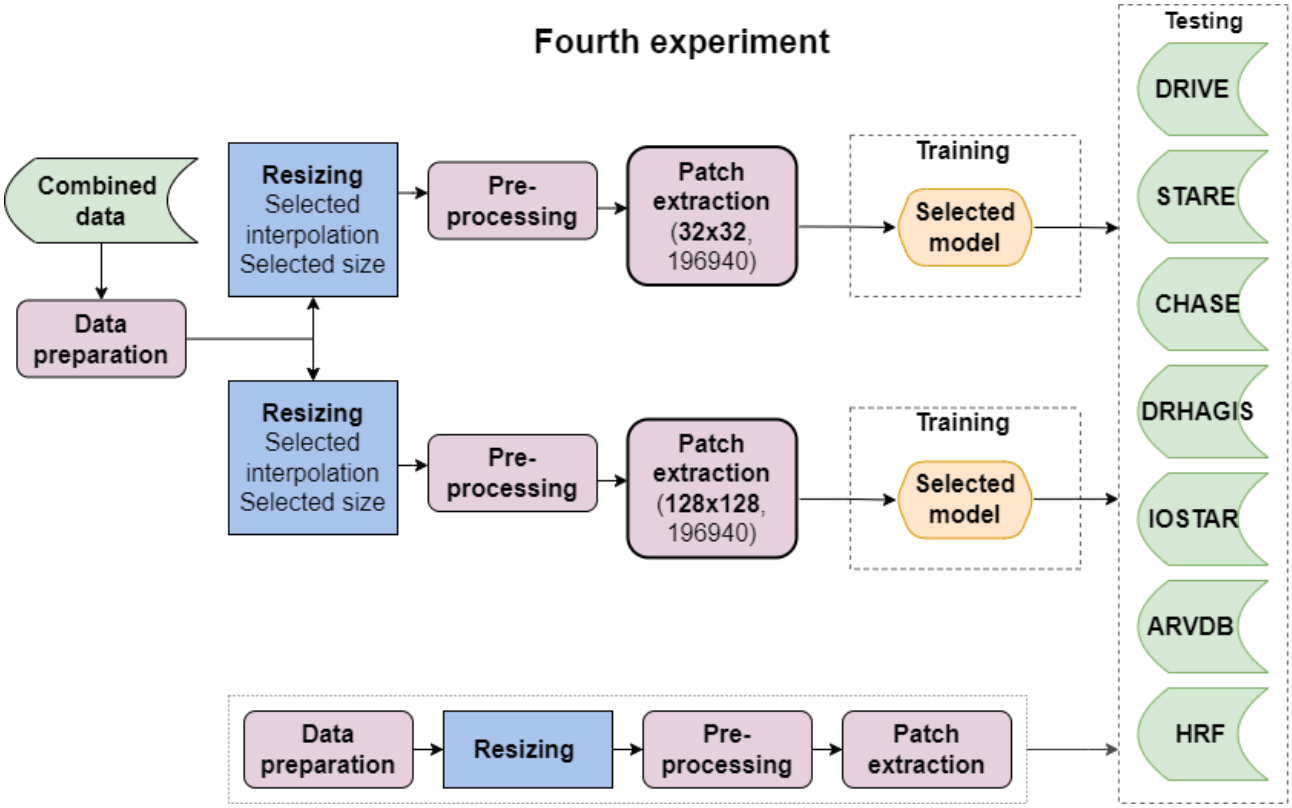

Figure 12. The scheme for input size selection

All conducted experiments provides information from different perspectives on several factors impact to DNN performance as well as advantages and disadvantages choosing these applications.

2.6. The evaluation of the DNNs

To evaluate the segmentation performance of models several evaluation metrics will be calculated. The confusion matrix will be produced and other metrics floating from it such as accuracy, sensitivity, specificity, precision, Area under the curve (AUC) and F1 score will be computed.

Confusion matrix can be computed only for binary segmentation as it gives 1 for the positive (vessel pixel) and 0 for negative (background pixel). Confusion matrix is presented in Table 4, where TP – true positive, FP – false positive, FN – false negative and TN – true negative. TP denotes a vessel pixel while TN – a background pixel, which were predicted by model and are annotated in ground truth. FP denotes a predicted vessel pixel which in the mask is annotated as a background while FN – a background pixel annotated as a vessel by observer.

Table 4. Confusion matrix

		Predicted value	
		1	0
Actual value	1	TP	FP
	0	FN	TN

Accuracy – a total number of correctly detected positives and negatives:

$$Accuracy = \frac{TP + TN}{TP + FN + FP + TN} \quad (4)$$

Sensitivity – correctly identified positives to all actual positives:

$$Sensitivity = \frac{TP}{TP + FN} \quad (5)$$

Specificity – correctly identified negatives to all actual negatives:

$$Specificity = \frac{TN}{TN + FP} \quad (6)$$

Precision – proportion of actual positives to all positives:

$$Precision = \frac{TP}{TP + FP} \quad (7)$$

F1 score or Dice coefficient (they are equal only in binary segmentation) – area of overlapping pixels divided by the total number of pixels:

$$F1 = \frac{2 * Precision * Sensitivity}{Precision + Sensitivity} \quad (8)$$

Area under the curve (AUC) is a metric also used to evaluate the segmentation results. The closer AUC value is to 1 – the better performance of the model.

For retinal vessels segmentation, achieving higher sensitivity and AUC score is more essential than achieving higher specificity (Kamran et al., 2021). As the key task of retinal vessel segmentation is to achieve the best segmentation of blood vessels, the main focus is on segmentation of vessel pixels (TP) than background (TN).

EXPERIMENTAL RESULTS

3.1. Model selection

As we are using images with different properties the most suitable model for diverse data needs to be selected. The most suitable algorithm is able to perform well and fast on retinal vessel segmentation. In order to compare BCDU-Net and ResUnet algorithms, both networks were trained on 200000 patches (size 64x64) of DRIVE dataset. Models were trained for 50 epochs. The algorithms were evaluated separately on all databases resizing them to the DRIVE size by nearest neighbour interpolation. All computations for this master thesis were done on VU MIF ITAPC supercomputer 3xNVIDIA DGX-1 Tesla V100 32GB graphic memory. The evaluations of the BCDU-Net and ResUnet performance on different datasets are presented in Table 5.

Table 5. Evaluation of BCDU-Net and ResUnet trained on DRIVE dataset

Dataset	Model	Accuracy	Sensitivity	Specificity	Precision	F1 score	AUC
DRIVE	BCDU-Net	**0.9550**	**0.8197**	0.9747	0.8257	**0.8227**	**0.9787**
	ResUnet	0.9543	0.7601	**0.9827**	**0.8650**	0.8092	0.9761
STARE	BCDU-Net	0.9476	**0.6420**	0.9752	0.7070	0.6729	**0.9476**
	ResUnet	**0.9505**	0.6090	**0.9824**	**0.7628**	**0.6773**	0.9457
CHASE_DB1	BCDU-Net	0.9386	**0.7450**	0.9590	0.6573	**0.6984**	**0.9536**
	ResUnet	**0.9411**	0.6832	**0.9684**	**0.6951**	0.6891	0.9456
DRHAGIS	BCDU-Net	0.9480	**0.8751**	0.9548	0.6444	0.7420	**0.9764**
	ResUnet	**0.9534**	0.8510	**0.9629**	**0.6818**	**0.7570**	0.9755
IOSTAR	BCDU-Net	0.9442	**0.8598**	0.9539	0.6823	**0.7608**	**0.9718**
	ResUnet	**0.9443**	0.8083	**0.9600**	**0.6996**	0.7500	0.9598
ARVDB	BCDU-Net	**0.9119**	**0.5529**	0.9849	0.8813	**0.6795**	**0.9312**
	ResUnet	0.9074	0.5089	**0.9885**	**0.8996**	0.6501	0.9295
HRF	BCDU-Net	0.9405	**0.8202**	0.9522	0.6257	0.7099	**0.9592**
	ResUnet	**0.9451**	0.7654	**0.9626**	**0.6661**	**0.7123**	0.9546

As seen from the Table 5, BCDU-Net achieved better sensitivity and AUC scores on all datasets compared to ResUnet. As we mentioned before, BCDU-Net was originally built and optimised on DRIVE dataset while ResUnet was originally created for different segmentation task. The predicted DRIVE image is shown in Figure 13.

Figure 13. Original image of DRIVE dataset (left) and BCDU-Net predicted blood vessels (right)

As it is seen in the figure, BCDU-Net was able to predict not only major vessels but thinner vessels also as they have a good contrast from the background and there is no huge noise in the image.
The highest sensitivity was achieved in the DRHAGIS dataset. It could be the outcome of resizing – as we mentioned in section 2.4., downscaling tends to remove pixels of the smallest vessels (especially in masks), which usually are the hardest task for DNNs to accurately segmentate from the images. As these smallest pixels are already lost in ground truths, the sensitivity increases as there are fewer positive pixels and they annotate larger vessels which model is able to catch. It also applies to other datasets which were downscaled but especially to the datasets which were resized to >= 2 times smaller size (HRF, IOSTAR, DRHAGIS). The segmented vasculature tree is shown in Figure 14.

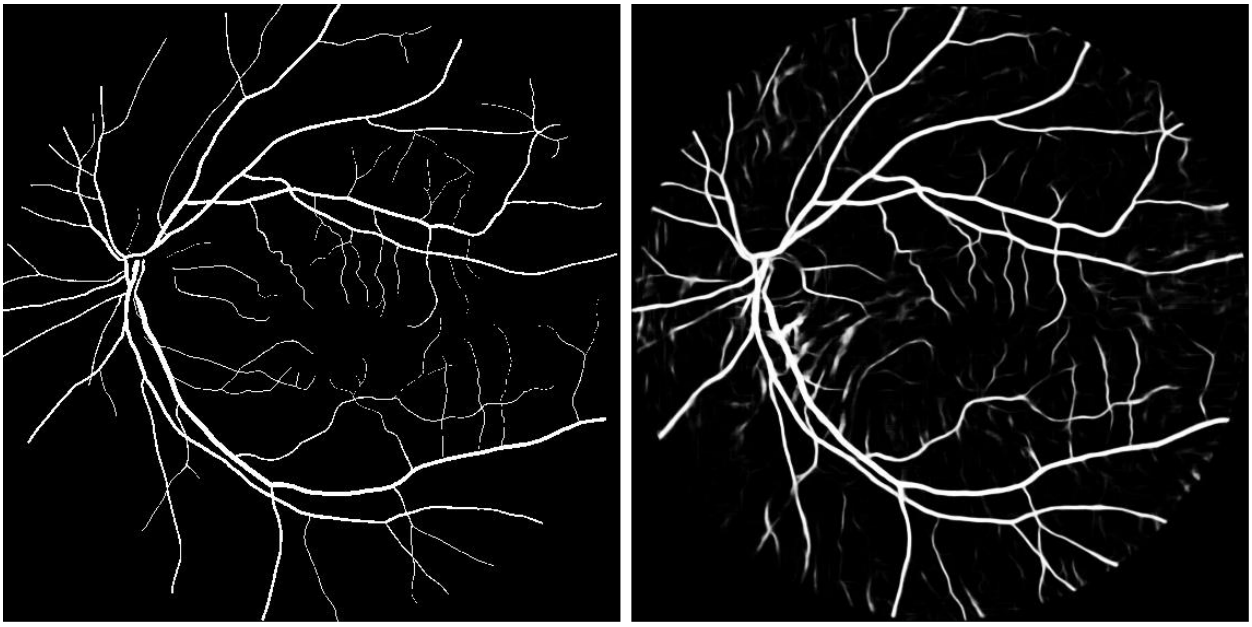

Figure 14. Ground truth (left) and BCDU-Net predicted vascular tree (right) from DRHAGIS dataset

Poor performance of BCDU-Net was observed on ARVDB database. The evaluation metrics for this dataset compared to other differs drastically. It achieved the highest specificity and very low sensitivity, meaning the poor segmentation of retinal vessels. The segmented vascular images have lots of noise, and not only thin but also major vessels were not accurately extracted (Figure 15).

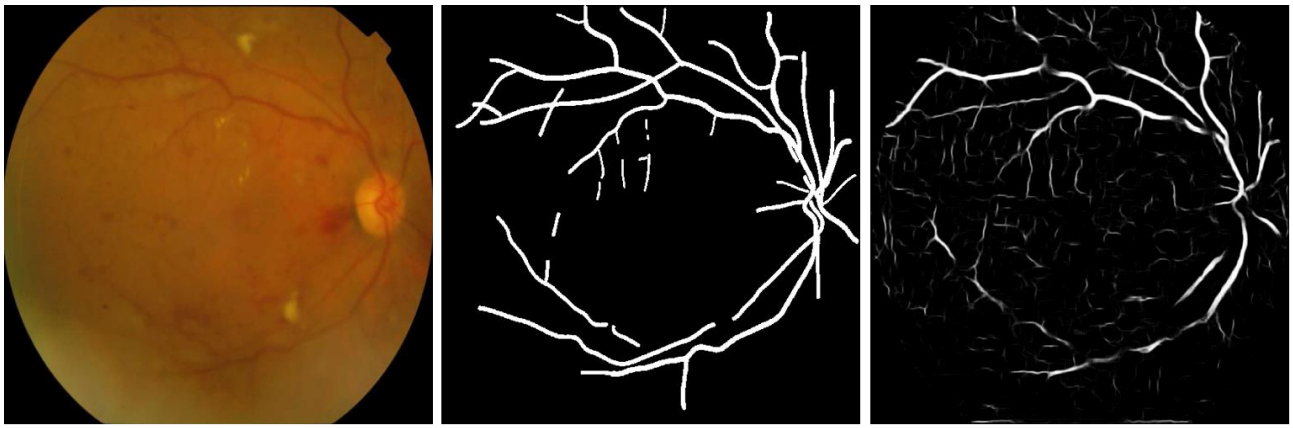

Figure 15. Original image (left), ground truth (middle) and BCDU-Net predicted vascular tree (right) from ARVDB dataset

The original image is blurred with uneven illumination and has a lot of lesions of various size. All these factors could influence the poor segmentation of retinal vessels.

As ResUnet produces poorer results in sensitivity and AUC on all datasets. It also achieved higher accuracy (except on DRIVE and ARVDB) on all datasets because of also higher specificity values. ResUnet segments background pixels better than BCDU-Net – vascular trees show less noise (Figure 16) but is unable to extract not only thin and tiny vessels but the major ones also.

Figure 16. ResUnet predicted vascular trees from DRIVE (left), DRHAGIS (middle) and ARVDB (right) datasets

As we need to chose the algorithm which is able to perform well on diverse data, both models were trained from scratch on combined data, resized to 565x565 with nearest neighbour interpolation from which 196490 (size 64x64) patches were extracted. ResUnet needed 5 times less time to learn as training speed was 62% faster than BCDU-Net. The performances of algorithms are present in Table 6.

Table 6. Evaluation of BCDU-Net and ResUnet trained on all data of size 565x565

Dataset	Model	Accuracy	Sensitivity	Specificity	Precision	F1 score	AUC
DRIVE	BCDU-Net	0.9525	0.7094	0.9880	**0.8961**	0.7919	0.9770
	ResUnet	**0.9539**	**0.7511**	**0.9835**	0.8693	**0.8059**	**0.9777**
STARE	BCDU-Net	**0.9663**	0.6998	**0.9912**	**0.8806**	0.7799	**0.9831**
	ResUnet	0.9650	**0.7461**	0.9854	0.8266	**0.7843**	0.9804
CHASE_DB1	BCDU-Net	**0.9611**	**0.8003**	0.9781	**0.7942**	**0.7972**	0.9612
	ResUnet	0.9599	0.7865	**0.9782**	0.7919	0.7892	**0.9799**
DRHAGIS	BCDU-Net	**0.9693**	0.8156	**0.9836**	**0.8229**	**0.8192**	**0.9866**
	ResUnet	0.9647	**0.8491**	0.9755	0.7636	0.8041	0.9841
IOSTAR	BCDU-Net	**0.9655**	**0.7781**	0.9871	0.8743	**0.8234**	**0.9861**
	ResUnet	0.9648	0.7662	**0.9877**	**0.8776**	0.8181	0.9852
ARVDB	BCDU-Net	0.9250	0.6741	0.9760	0.8512	0.7524	0.9562
	ResUnet	**0.9275**	**0.6928**	0.9752	0.8506	**0.7636**	**0.9606**
HRF	BCDU-Net	**0.9633**	0.7624	**0.9828**	**0.8120**	**0.7864**	**0.9756**
	ResUnet	0.9606	**0.7865**	0.9775	0.7730	0.7797	0.9733

ResUnet reached 2.8%-6.6% better sensitivity scores in all datasets (except IOSTAR and CHASE_DB1), especially on DRIVE and STARE datasets, which sensitivity values were higher by 5.8% and 6.6% respectively compared to BCDU-Net. BCDU-Net trained on all data, could not perform so well as previously on DRIVE dataset – sensitivity decreased by 13.5%, F1 score – 3.8%. ResUnet trained on combined data performed quite similar on DRIVE dataset, and much better on other datasets compared when it was trained only on DRIVE. The ResUnet sensitivity on ARVDB increased by 26.5% (while BCDU-Net – 18%).

ResUnet was selected for further segmentations of retinal vessels as it is able to perform better, faster and more stable on combined data.

3.2. Size selection

As our data consists images of various sizes another experiment is done in order to select the most appropriate size which would achieve the best segmentation of retinal blood vessels without loosing too much information because of resizing. Combined data (with its origin dimensions) was resized with nearest neighbour interpolation to the sizes of 750x750 and 1000x1000. From resized images 196490 patches (size 64x64) were extracted and ResUnet was trained from scratch for 50 epochs each time. The training time of the algorithm does not change, but it requires much more memory resources to handle 1.5-2 times bigger files as it consists data of larger size. The performances are shown in Table 7.

Table 7. ResUnet performance on all data of different sizes

Dataset	Image size	Accuracy	Sensitivity	Specificity	Precision	F1 score	AUC
DRIVE	565x565	**0.9539**	**0.7511**	0.9835	0.8693	**0.8059**	**0.9777**
	750x750	0.9518	0.6965	0.9890	0.9025	0.7862	0.9776
	1000x1000	0.9493	0.6643	**0.9909**	**0.9142**	0.7695	0.9771
STARE	565x565	**0.9650**	**0.7461**	0.9854	0.8266	**0.7843**	0.9804
	750x750	0.9642	0.6517	0.9934	**0.9024**	0.7568	**0.9821**
	1000x1000	0.9621	0.6243	**0.9937**	0.9021	0.7379	0.9782
CHASE_DB1	565x565	0.9599	**0.7865**	0.9782	0.7919	**0.7892**	0.9799
	750x750	**0.9601**	0.7506	**0.9822**	**0.8163**	0.7821	**0.9802**
	1000x1000	0.9583	0.7309	**0.9822**	0.8127	0.7696	0.9778
DRHAGIS	565x565	0.9647	**0.8491**	0.9755	0.7636	0.8041	0.9841
	750x750	**0.9680**	0.8157	**0.9823**	**0.8113**	**0.8135**	**0.9860**
	1000x1000	0.9674	0.8130	0.9818	0.8065	0.8098	0.9844
IOSTAR	565x565	**0.9648**	**0.7662**	0.9877	0.8776	**0.8181**	0.9852
	750x750	0.9644	0.7411	0.9901	0.8956	0.8111	**0.9858**
	1000x1000	0.9639	0.7327	**0.9906**	**0.8996**	0.8076	0.9851
ARVDB	565x565	**0.9275**	**0.6928**	0.9752	0.8506	**0.7636**	0.9606
	750x750	0.9267	0.6740	0.9781	0.8622	0.7566	**0.9614**
	1000x1000	0.9228	0.6319	**0.9820**	**0.8772**	0.7346	0.9578
HRF	565x565	0.9606	**0.7865**	0.9775	0.7730	0.7797	0.9733
	750x750	**0.9645**	0.7456	**0.9858**	**0.8360**	**0.7882**	**0.9780**
	1000x1000	0.9626	0.7516	0.9832	0.8128	0.7810	0.9762

As we can see, when the size of the image is increasing – the sensitivity decreases by 2.7%-16.3% in all datasets, but especially for DRIVE and STARE datasets, whose images were upscaled. Nearest neighbour interpolation creates blocky pixels which reduces model ability to accurately extract vessels as it gets not only normal but also artificially created pixels. When image size increased, the sensitivity for STARE dataset decreased the most: with size of 750x750 – by 12,6% and with size of 1000x1000 – by 16,3%, compared to the size of 565x565. Even though, the highest AUC score was achieved in 750x750 size. The example of segmented STARE image is presented in Figure 17.

Figure 17. The segment of image (left), ground truth (middle) and predicted vessels (right) from STARE dataset (size 750x750)

As we mentioned before, by downscaling large images to the size of 565x565, a lot of pixels of small vessels were lost, especially in ground truths. It produces higher sensitivity values as only bigger pixels are left in masks. These pixels represents larger features in the images which model is able to segmentate. When masks from DRHAGIS and HRF were resized to 750x750 and 1000x1000, fewer small vessels lost their details and more precise evaluation is possible. The example is shown in Figure 18.

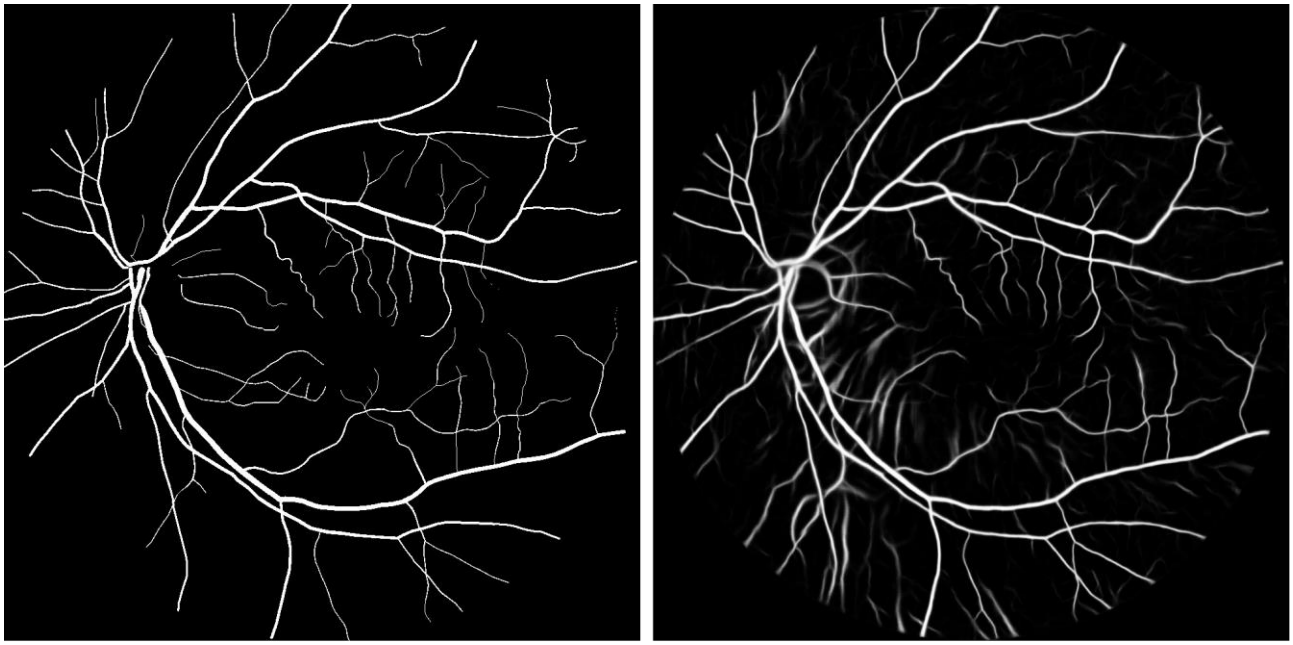

Figure 18. The mask (left) and predicted vascular tree (right) from DRHAGIS dataset (size 1000x1000)

Even though the segmentation of major and small vessels is quite good, model segmented both retinal and choroidal vessels, making the image noisy with a lot unnecessary and not relevant information.

The AUC score increased for all datasets when images were resized to the size of 750x750 (except DRIVE, which value differs with third decimal point) compared to sizes 565x565 and 1000x1000.

As we are trying to preserve the most truthful retinal vessel segmentation without loosing much information, it was decided to conduct further experiments with images of the 750x750 size.

3.3. Interpolation selection

As in previous experiments our focus was on choosing a better model and sizes for data with various dimensions and properties – the fastest interpolation method was used for resizing. This experiment was conducted in order to analyse the influence of the interpolation method for segmentation of retinal vessels. Combined data (with its origin dimensions) was resized by bilinear and bicubic interpolations to the size of 750x750, from which 196490 patches (size 64x64) were extracted and model was trained for 50 epochs from scratch. The ResUnet performance on differently interpolated data is present in Table 8, where 'nearest neigh' is for nearest neighbour interpolation.

Table 8. ResUnet performance on all data resized by different interpolations

Dataset	Interpolation	Accuracy	Sensitivity	Specificity	Precision	F1 score	AUC
DRIVE	Nearest neigh	0.9518	0.6965	0.9890	0.9025	0.7862	0.9776
	Bilinear	**0.9521**	**0.7047**	0.9880	0.8943	**0.7883**	**0.9777**
	Bicubic	0.9441	0.6071	**0.9936**	**0.9337**	0.7355	0.9765
STARE	Nearest neigh	**0.9642**	0.6517	**0.9934**	**0.9024**	0.7568	**0.9821**
	Bilinear	0.9659	**0.7127**	0.9895	0.8639	**0.7810**	0.9814
	Bicubic	0.9631	0.6416	0.9931	0.8963	0.7478	0.9792
CHASE_DB1	Nearest neigh	0.9601	0.7506	0.9822	0.8163	**0.7821**	0.9802
	Bilinear	0.9588	**0.7577**	0.9799	0.7990	0.7778	0.9786
	Bicubic	**0.9606**	0.7332	**0.9846**	**0.8338**	0.7802	**0.9803**
DRHAGIS	Nearest neigh	0.9680	0.8157	0.9823	0.8113	**0.8135**	0.9860
	Bilinear	0.9662	**0.8258**	0.9793	0.7886	0.8068	0.9847
	Bicubic	**0.9687**	0.7786	**0.9865**	**0.8432**	0.8096	**0.9864**
IOSTAR	Nearest neigh	**0.9644**	0.7411	0.9901	0.8956	**0.8111**	0.9858
	Bilinear	0.9642	**0.7418**	0.9899	0.8940	0.8108	0.9857
	Bicubic	0.9640	0.7279	**0.9912**	**0.9045**	0.8066	**0.9859**
ARVDB	Nearest neigh	**0.9267**	**0.6740**	0.9781	0.8622	**0.7566**	**0.9614**
	Bilinear	0.9265	0.6684	**0.9788**	0.8647	0.7540	0.9608
	Bicubic	0.9244	0.6496	0.9800	**0.8683**	0.7432	0.9584
HRF	Nearest neigh	**0.9645**	0.7456	0.9858	0.8360	**0.7882**	0.9780
	Bilinear	0.9634	**0.7600**	0.9832	0.8147	0.7864	0.9771
	Bicubic	0.9642	0.7187	**0.9881**	**0.8550**	0.7809	**0.9783**

Using bilinear interpolation, sensitivity increased by 1.9%-16.1% for all datasets (except ARVDB) and significantly for STARE dataset compared to nearest neighbour and bicubic interpolations. It also achieved lowest precision and specificity scores (except ARVDB). Similar accuracy, F1 and AUC scores was achieved as with nearest neighbour interpolation. Using bicubic interpolation, sensitivity decreased by 1.8%-13.8% for all datasets and extremely for DRIVE dataset compared to other resizing techniques (by 13.8% comparing to bilinear interpolation and by 12.8% compared to nearest neighbour interpolation). Nevertheless, it achieved highest AUC scores for high quality images (HRF, IOSTAR, DRHAGIS and CHASE_DB1), but it did not significantly differed from results of other interpolations. As we shown before, bilinear and bicubic interpolations provided similar results in pixels, but bilinearly interpolated images were more blurred. As all images were pre-processed by the same techniques, without individually improvements (as some images are more blurred, noisy, etc.), bilinear interpolation was the most favourable one as blurred effect reduced noise in images and model performed better. The example is shown in Figure 19.

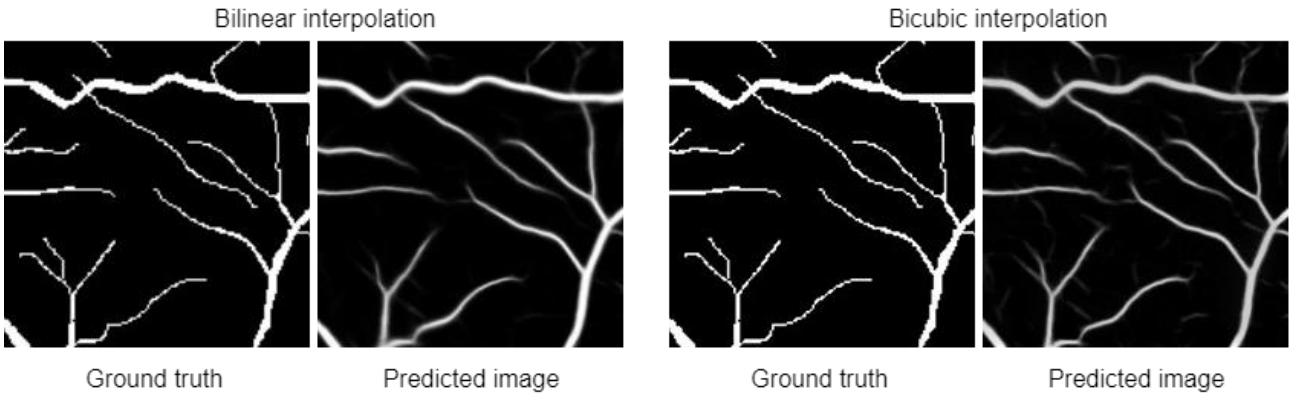

Figure 19. The segments of masks and predicted images from DRIVE dataset

Due to significantly increased sensitivity scores bilinear interpolation was chosen as the most suitable technique when resizing images of different quality.

3.4. Input size selection

The last experiment was done in order to choose the best input size which would achieve better segmentation results. In all prior tests patches of size 64x64 were input for the model. As we mentioned before, different input size have different amount of information from which model decides. Because of that, in this experiment combined data was resized by bilinear interpolation to the size of 750x750 from which 196490 patches of sizes 32x32 and 128x128 were extracted and put into the ResUnet. As usually, model was trained from scratch for 50 epochs and evaluated on all datasets. With input size of 32x32, model training time decreased by 52.4% compared to the input

size of 64x64, while input size of 128x128 prolonged training time by 69.2% compared to the input size of 64x64. The segmentation results are present in Table 9.

Table 9. Input size impact to ResUnet performance

Dataset	Input size	Accuracy	Sensitivity	Specificity	Precision	F1 score	AUC
DRIVE	32x32	0.9480	0.6452	**0.9918**	**0.9191**	0.7582	0.9764
	64x64	0.9521	0.7047	0.9880	0.8943	0.7883	**0.9777**
	128x128	**0.9533**	**0.7672**	0.9802	0.8487	**0.8059**	0.9775
STARE	32x32	0.9637	0.6510	**0.9929**	**0.8946**	0.7537	0.9752
	64x64	**0.9659**	0.7127	0.9895	0.8639	0.7810	0.9814
	128x128	**0.9659**	**0.7912**	0.9822	0.8054	**0.7982**	**0.9833**
CHASE_DB1	32x32	0.9553	0.7002	**0.9822**	**0.8054**	0.7491	0.9745
	64x64	**0.9588**	0.7577	0.9799	0.7990	0.7778	0.9786
	128x128	0.9579	**0.8229**	0.9721	0.7565	**0.7883**	**0.9799**
DRHAGIS	32x32	0.9655	0.8224	0.9788	0.7838	0.8026	0.9832
	64x64	**0.9662**	0.8258	**0.9793**	**0.7886**	**0.8068**	**0.9847**
	128x128	0.9613	**0.8765**	0.9692	0.7262	0.7943	0.9846
IOSTAR	32x32	0.9625	0.7257	0.9898	0.8911	0.8000	0.9832
	64x64	**0.9642**	0.7418	**0.9899**	**0.8940**	0.8108	**0.9857**
	128x128	0.9641	**0.7739**	0.9860	0.8644	**0.8167**	0.9856
ARVDB	32x32	0.9162	0.5704	**0.9863**	**0.8939**	0.6964	0.9506
	64x64	0.9265	0.6684	0.9788	0.8647	0.7540	**0.9608**
	128x128	**0.9277**	**0.6921**	0.9755	0.8511	**0.7634**	0.9607
HRF	32x32	0.9617	0.7484	0.9824	0.8054	0.7759	0.9744
	64x64	**0.9634**	0.7600	**0.9832**	**0.8147**	**0.7864**	**0.9771**
	128x128	0.9579	**0.8133**	0.9720	0.7385	0.7741	0.9740

With input size of 32x32, sensitivity and F1 scores drastically decreased for images of poorer quality (DRIVE, STARE, CHASE_DB1, ARVDB), and not so significantly for other datasets compared to the input size of 64x64. With input size of 32x32, the highest specificity and precision scores were achieved for poorer quality images (DRIVE, STARE, CHASE_DB1, ARVDB), while with input size o 64x64 - for high quality images. With input size of 128x128, sensitivity highly increased for all datasets compared to the input size of 64x64. Comparing 128x128 between 32x32 input size, for the input of 128x128 size, sensitivity for datasets increased by: STARE – 21,5%, ARVDB – 21,3%, DRIVE – 18,9%, CHASE_DB1 – 17,5%, HRF – 8,7%, DRHAGIS and IOSTAR – 6,6%. The difference of predicted vascular trees when input size is 32x32 and 128x128 is present in Figure 20.

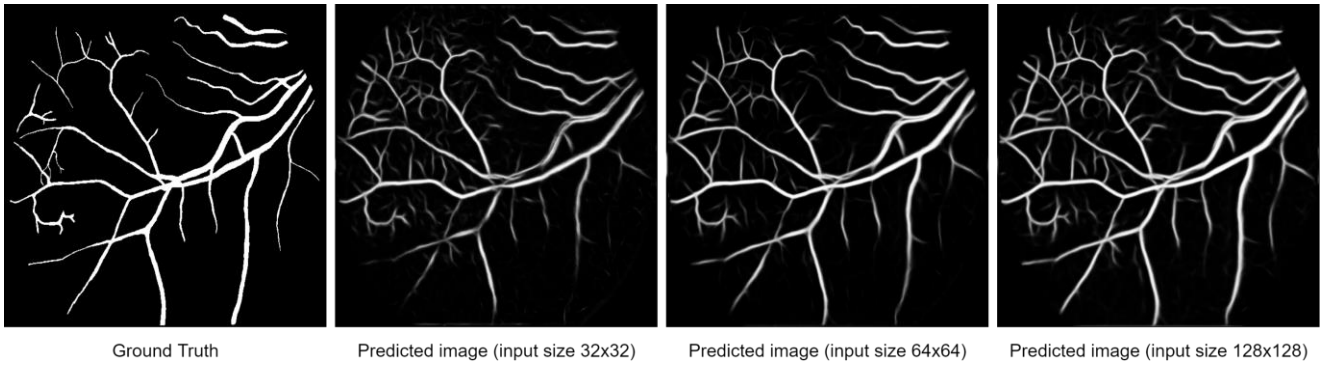

Figure 20. The impact of input size to retinal vessel segmentation (STARE)

As we can see in the figure, model is not able to predict even major vessels when the size of the input is 32x32. With larger input size, both major and small blood vessels are segmented more accurately and precise. Furthermore, we observed that increased input size lets model to distinguish vessels from background noise more accurately and in the area of OD separate uneven border colour from vessels (Figure 21).

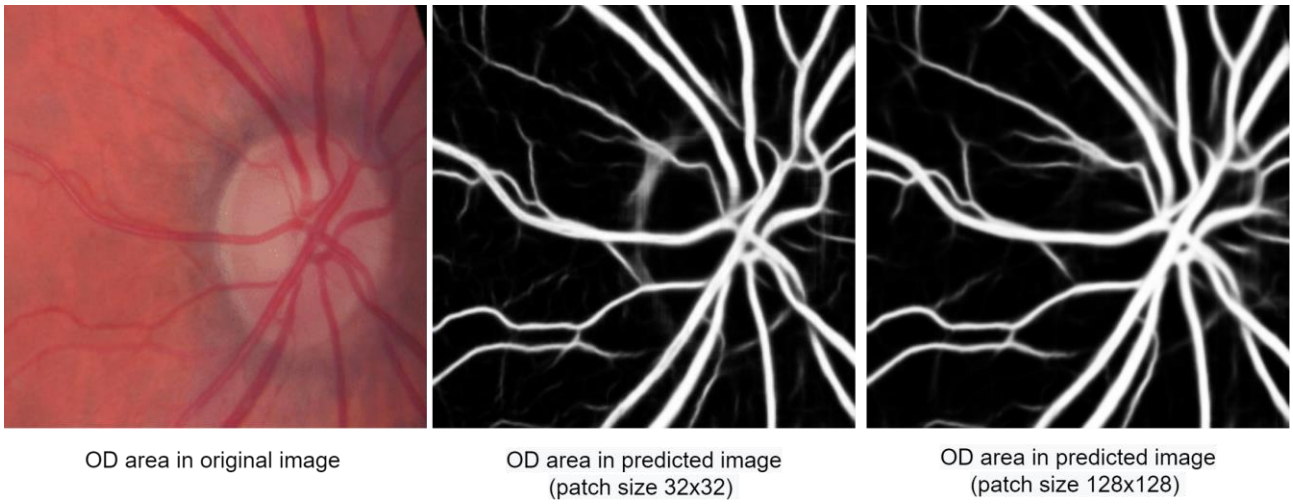

Figure 21. The impact of input size for differentiation of relevant information (DRHAGIS)

Larger input size gives more contextual information to the model and enables proper segmentation of retinal blood vessels.

To conclude all experiment results, ResUnet performed better on diverse data compared to BCDU-Net and achieved the best segmentation of retinal vessels when images were resized by bilinear interpolation to the size of 750x750 with patch extraction of 128x128 size.

DISCUSSION

4.1. Model selection

As the development of deep learning methods increases rapidly, there are a lot of proposed models to conduct retinal vessel segmentation. As we explained before, BCDU-Net and ResUnet were chosen due to their suggested abilities to perform well on diverse data as well as some structural similarities within algorithms. As both algorithms were proposed only on DRIVE datasets, we evaluated their performance on other datasets when models are trained on DRIVE images. BCDU-Net outperformed ResUnet as reached higher sensitivity and AUC scores in all datasets.

As we mentioned prior, usually algorithms are optimised for a dataset of specific characteristics. Because of that, we decided to combine training images from all seven datasets into combined data, which would contain images of different quality and properties – creating heterogeneous data and simulating real-life cases. The approach of merging different images was done by Hacisoftaoglu et al. (2020) for the classification task to distinguish of DR and healthy images where researchers observed that diverse images improved the accuracy of DR detection. The datasets suitable for unsupervised models were used. We could not find any study where fundus images of various datasets were combined for a supervised retinal vessel segmentation task. This master thesis proposes novelty as training images from seven used datasets were combined into one diverse training data in order to represent and analyse the different quality and properties that impact the performance of the model.

Original training images were resized to the size of the DRIVE dataset and both models were trained from scratch on combined data. This time ResUnet was superior to BCDU-Net – performed much faster and better by achieving higher sensitivity values for mostly all datasets indicating its capabilities to analyse diverse data better. Because of that ResUnet and combined data were selected for other experiments. By combining data, accuracy, sensitivity and AUC increased for the majority of datasets. This experiment also shows that diversity of features improves the model ability to produce more precise segmentation of retinal vessels. Galdran et al. (2022) stated that DRIVE dataset images are still used as the main dataset for algorithm construction and other less known datasets of higher quality are ignored due to scholars efforts to compare results to prior researches. We want to add that by using DRIVE as the main dataset for training, other datasets of larger size loose a lot of valuable information about the condition of small vessels due to resizing. These models used for real-life applications could provide untruthful results when larger images are extremely resized.

4.2. Size selection

As we already stressed out that small image size is unfavourable for larger images due to the loss of important information about smaller vessels, the various image sizes were considered to preserve as much as possible information. Original training images were resized to 1.5 and 2 times bigger sizes than the size of the DRIVE dataset. Increased size of the images produced lower sensitivity and F1 scores basically for all datasets. As we argued before, we think that it is a more truthful representation of larger image segmentation as ground truths maintain a larger amount of small vessels pixels. Upscaled images may confuse models due to artificially created pixels leading the models to perform poorer. Because of that images should not be upscaled by huge volumes. Further studies may consider excluding images of the smallest size. Despite that, the highest AUC scores were observed when the size was increased by 1.5 points and the size of 750x750 was selected for other experiments. Rukundo (2021) evaluated the effects of image size on U-net segmentation of myocardial infarction in magnetic resonance imaging. These images from one dataset of size 128x128 were increased 2 times to the size of 256x256 and U-net performed better. Our images contrastingly to mentioned study are combined from various datasets and some images had to be upscaled while others were downscaled. Horwath et al. (2020) observed that segmentation improved on high quality images when convolutional kernel size is increased, but a number of trainable parameters also increases which prolongs the training time. The prolonged training time when image size is increased was observed in our work. However, we did not analyse which structural changes in the model favourites different quality images and further studies could be conducted in this area.

4.3. Interpolation selection

The effects of three interpolations on segmentation performance were evaluated. The highest sensitivity scores were achieved with bilinear interpolation almost for all datasets. We think it is because the same pre-processing was done on all images despite their quality. For further studies we suggest performing pre-processing more individually without generalising it on different quality images (improve features of low quality images more). the Bilinear interpolation creates a blurred effect on images and low quality images with high noise could benefit from this interpolation parallelly improving segmentation results. For the same reason, bicubic interpolation could be the most unfavourable to the images of low quality as it produces quite sharp images. Bicubic interpolation scored the highest AUC scores in images of high quality. Nevertheless, bilinear interpolation was selected due to the low sensitivity scores of bicubic interpolation. Triwijoyo and Adil (2021) also used the same interpolation methods for MESSIDOR (Methods to evaluate segmentation and indexing techniques in the field of retinal ophthalmology) dataset which contains 1200 images of different sizes and is used in unsupervised retinal vessel segmentation as it does not contains ground truths. The dimensions of images were downscaled 3.75-9 times to the size 256x256 and bicubic

interpolation was considered the most favourable compared to other interpolations. Our research analyses not only downscaling impact on the segmentation results but upscaling also. Also, we avoided downscaling to such small values in order to preserve valuable information and did not evaluated different interpolations effects on such sizes. In addition, as we mentioned downscaling removes a lot of information and downscaling by extreme volumes should be avoided in order to have reliable retinal vessel segmentation.

4.4. Input size selection

As mentioned before, CNNs can process inputs of arbitrary size, but the inputs of different scales represent different contextual information to the models. Our findings show that a larger input size increases the accuracy and F1 score for low quality images and the sensitivity of significant values for all images. AUC scores are almost the same for both inputs of sizes 64x64 and 128x128. We suggest that contextual information provides important insights from which the model is able to predict better and a larger input size enables the greater performance of retinal vessel segmentation. Despite that, it also requires higher memory resources and extends training time. Sekou et al. (2019) state that patch based methods need a sufficient amount of discriminative information for effective retinal segmentation of retinal vessels. It agrees with our argument of contextual information importance and we can state that the smallest input made the model perform poorly due to the lack of surrounding details. Richter et al. (2021) suggest that each algorithm has a preferred input size without a direct connection between a larger input size and better model performance. In addition, they show that the structure of the model must match with image properties for effective model performance and residual connections successfully help in counteracting mismatches. We do not rule out such a possibility as our algorithm consists of many residual connections and further studies on input size effects for other models could give a clearer view. Hamwood et al.(2018) suggest that large patch input increases CNN classification accuracy on optical coherence tomography images. Our findings complement this idea that a larger size of patch increases not only accuracy but sensitivity also of retinal vessel segmentation from fundus images.

In conclusion, this master thesis analyses seven datasets of fundus images with different quality and their effects with attention to image properties on the model performance on retinal vessel segmentation. To conclude our work, we show that models built on one dataset do not provide reliable retinal vessel segmentation on images of various characteristics and handle diverse data differently. This master thesis shows that resizing affects heterogeneous data deeply and huge image size alterations should be avoided in order to maintain the highest amount of information for retinal vessel segmentation. Also, our work suggests that bilinear interpolation improves segmentation performance on generally pre-processed diverse data. In the end, our master thesis

suggests that a larger input size gives greater contextual information to the model and segmentation of retinal vessels improves.

CONCLUSIONS

1. ResUnet trained on combined data achieved 2.8%-6.6% higher sensitivity values for the majority of datasets and performs better than BCDU-Net on images with different quality.
2. Image size of 750x750 provided the highest AUC results on all datasets when ResUnet is trained on combined data but sizes of 750x750 and 1000x1000 decreased sensitivity scores by 2.7%-16.3% for images of all qualities.
3. Bilinear interpolation achieved 1.9%-16.1% higher sensitivity values while bicubic interpolation scored 1.8%-13.8% lower sensitivity values for all quality images compared to other interpolations.
4. The input size of 128x128 for ResUnet achieved 17.5%-21.5% higher sensitivity values on low quality images and 6.6%-8.7% sensitivity scores on high quality images compared to input sizes of 32x32 and 64x64.

ACKNOWLEDGEMENTS

I would like to acknowledge and express my deepest gratitude to my supervisor dr. Jolita Bernatavičienė who spent a tremendous amount of time for constant guiding, suggesting improvements and sharing her knowledge with me. I also want to thank you for a regular interactions and comprehensive assistance in all encountered difficulties from the very beginning of this master thesis to the very end.

I want to thank dr. Povilas Treigys for introduction to deep learning and provided guidelines after reviewing research progress, all technical support and time spent debugging my algorithms and various errors.

I want to thank Ričardas Toliušis for the introduction to the codes of retinal vessel segmentation.

I want to thank my groupmates for their constant emotional support and company throughout these years.

The authors thank the Information Technology Open Access Center of the Faculty of Mathematics and Informatics of Vilnius University for the HPC resources provided for the calculations of this work and support team for providing fast support to all queries.

REFERENCES

1. Abbasi-Sureshjani, S., Smit-Ockeloen, I., Zhang, J., Ter Haar Romeny, B., 2015. Biologically-Inspired Supervised Vasculature Segmentation in SLO Retinal Fundus Images, in: Kamel, M., Campilho, A. (Eds.), Image Analysis and Recognition, Lecture Notes in Computer Science. Springer International Publishing, Cham, pp. 325–334. https://doi.org/10.1007/978-3-319-20801-5_35
2. Abdulsahib, A.A., Mahmoud, M.A., Aris, H., Gunasekaran, S.S., Mohammed, M.A., 2022. An Automated Image Segmentation and Useful Feature Extraction Algorithm for Retinal Blood Vessels in Fundus Images. Electronics 11, 1295. https://doi.org/10.3390/electronics11091295
3. Abdulsahib, A.A., Mahmoud, M.A., Mohammed, M.A., Rasheed, H.H., Mostafa, S.A., Maashi, M.S., 2021. Comprehensive review of retinal blood vessel segmentation and classification techniques: intelligent solutions for green computing in medical images, current challenges, open issues, and knowledge gaps in fundus medical images. Netw Model Anal Health Inform Bioinforma 10, 20. https://doi.org/10.1007/s13721-021-00294-7
4. Abràmoff, M.D., Garvin, M.K., Sonka, M., 2010. Retinal Imaging and Image Analysis. IEEE Rev Biomed Eng 3, 169–208. https://doi.org/10.1109/RBME.2010.2084567
5. Adapa, D., Joseph Raj, A.N., Alisetti, S.N., Zhuang, Z., K, G., Naik, G., 2020. A supervised blood vessel segmentation technique for digital Fundus images using Zernike Moment based features. PLoS One 15, e0229831. https://doi.org/10.1371/journal.pone.0229831
6. Akram, M.U., Akbar, S., Hassan, T., Khawaja, S.G., Yasin, U., Basit, I., 2020. Data on fundus images for vessels segmentation, detection of hypertensive retinopathy, diabetic retinopathy and papilledema. Data in Brief 29, 105282. https://doi.org/10.1016/j.dib.2020.105282
7. Atli, İ., Gedik, O.S., 2021. Sine-Net: A fully convolutional deep learning architecture for retinal blood vessel segmentation. Engineering Science and Technology, an International Journal 24, 271–283. https://doi.org/10.1016/j.jestch.2020.07.008
8. Azad, R., Asadi, M., Fathy, M., Escalera, S., 2019. Bi-Directional ConvLSTM U-Net with Densley Connected Convolutions. pp. 406–415. https://doi.org/10.1109/ICCVW.2019.00052
9. Boudegga, H., Elloumi, Y., Akil, M., Hedi Bedoui, M., Kachouri, R., Abdallah, A.B., 2021. Fast and efficient retinal blood vessel segmentation method based on deep learning network. Computerized Medical Imaging and Graphics 90, 101902. https://doi.org/10.1016/j.compmedimag.2021.101902
10. Bovik, A.C., 2009. Chapter 3 - Basic Gray Level Image Processing, in: Bovik, A. (Ed.), The Essential Guide to Image Processing. Academic Press, Boston, pp. 43–68. https://doi.org/10.1016/B978-0-12-374457-9.00003-2
11. Budai, A., Bock, R., Maier, A., Hornegger, J., Michelson, G., 2013. Robust Vessel Segmentation in Fundus Images [WWW Document]. International Journal of Biomedical Imaging. https://doi.org/10.1155/2013/154860
12. Chalakkal, R.J., Abdulla, W., 2017. Automatic segmentation of retinal vasculature, in: 2017 IEEE International Conference on Acoustics, Speech and Signal Processing (ICASSP). Presented at the 2017 IEEE International Conference on Acoustics, Speech and Signal Processing (ICASSP), pp. 886–890. https://doi.org/10.1109/ICASSP.2017.7952283
13. Chalakkal, R.J., Abdulla, W.H., Thulaseedharan, S.S., 2019. Quality and content analysis of fundus images using deep learning. Computers in Biology and Medicine 108, 317–331. https://doi.org/10.1016/j.compbiomed.2019.03.019
14. Chen, C., Chuah, J.H., Ali, R., Wang, Y., 2021. Retinal Vessel Segmentation Using Deep Learning: A Review. IEEE Access 9, 111985–112004. https://doi.org/10.1109/ACCESS.2021.3102176
15. Cheng, Y., Ma, M., Zhang, L., Jin, C., Ma, L., Zhou, Y., 1 School of Biomedical Engineering, Sun Yat-sen University, Guangzhou 510006, China, 2 Zhongshan Ophthalmic Center, Sun

Yat-sen University, Guangzhou 510006, China, 3 Department of Medical Informatics, Zhongshan School of Medicine, Sun Yat-sen University, Guangzhou 510006, China, †These authors contributed equally to this work., 2020. Retinal blood vessel segmentation based on Densely Connected U-Net. Mathematical Biosciences and Engineering 17, 3088–3108. https://doi.org/10.3934/mbe.2020175
16. Costa, P., Campilho, A., Hooi, B., Smailagic, A., Kitani, K., Liu, S., Faloutsos, C., Galdran, A., 2017. EyeQual: Accurate, Explainable, Retinal Image Quality Assessment, in: 2017 16th IEEE International Conference on Machine Learning and Applications (ICMLA). Presented at the 2017 16th IEEE International Conference on Machine Learning and Applications (ICMLA), pp. 323–330. https://doi.org/10.1109/ICMLA.2017.0-140
17. Dai, G., He, W., Xu, L., Pazo, E.E., Lin, T., Liu, S., Zhang, C., 2020. Exploring the effect of hypertension on retinal microvasculature using deep learning on East Asian population. PLoS One 15, e0230111. https://doi.org/10.1371/journal.pone.0230111
18. Ehrlich, R., Harris, A., Wentz, S.M., Moore, N.A., Siesky, B.A., 2017. Anatomy and Regulation of the Optic Nerve Blood Flow☆, in: Reference Module in Neuroscience and Biobehavioral Psychology. Elsevier. https://doi.org/10.1016/B978-0-12-809324-5.01301-8
19. Galdran, A., Anjos, A., Dolz, J., Chakor, H., Lombaert, H., Ayed, I.B., 2022. State-of-the-art retinal vessel segmentation with minimalistic models. Sci Rep 12, 6174. https://doi.org/10.1038/s41598-022-09675-y
20. Gao, S., Gruev, V., 2011. Bilinear and bicubic interpolation methods for division of focal plane polarimeters. Opt. Express, OE 19, 26161–26173. https://doi.org/10.1364/OE.19.026161
21. Gao, X., Cai, Y., Qiu, C., Cui, Y., 2017. Retinal blood vessel segmentation based on the Gaussian matched filter and U-net, in: 2017 10th International Congress on Image and Signal Processing, BioMedical Engineering and Informatics (CISP-BMEI). Presented at the 2017 10th International Congress on Image and Signal Processing, BioMedical Engineering and Informatics (CISP-BMEI), pp. 1–5. https://doi.org/10.1109/CISP-BMEI.2017.8302199
22. Ghosh, S., Das, N., Das, I., Maulik, U., 2019. Understanding Deep Learning Techniques for Image Segmentation. arXiv:1907.06119 [cs].
23. Gonzalez, R.C., Woods, R.E., 2018. Digital image processing, Fourth edition. ed. Pearson, New York, NY.
24. Guo, C., Szemenyei, M., Yi, Y., Wang, W., Chen, B., Fan, C., n.d. SA-UNet: Spatial Attention U-Net for Retinal Vessel Segmentation 7.
25. Hacisoftaoglu, R.E., Karakaya, M., Sallam, A.B., 2020. Deep Learning Frameworks for Diabetic Retinopathy Detection with Smartphone-based Retinal Imaging Systems. Pattern Recognit Lett 135, 409–417. https://doi.org/10.1016/j.patrec.2020.04.009
26. Hamwood, J., Alonso-Caneiro, D., Read, S.A., Vincent, S.J., Collins, M.J., 2018. Effect of patch size and network architecture on a convolutional neural network approach for automatic segmentation of OCT retinal layers. Biomed. Opt. Express, BOE 9, 3049–3066. https://doi.org/10.1364/BOE.9.003049
27. Hemelings, R., Elen, B., Stalmans, I., Van Keer, K., De Boever, P., Blaschko, M.B., 2019. Artery–vein segmentation in fundus images using a fully convolutional network. Computerized Medical Imaging and Graphics 76, 101636. https://doi.org/10.1016/j.compmedimag.2019.05.004
28. Hernandez-Matas, C., Argyros, A.A., Zabulis, X., 2019. Retinal image preprocessing, enhancement, and registration, in: Computational Retinal Image Analysis. Elsevier, pp. 59–77. https://doi.org/10.1016/B978-0-08-102816-2.00004-6
29. Holm, S., Russell, G., Nourrit, V., McLoughlin, N., 2017. DR HAGIS-a fundus image database for the automatic extraction of retinal surface vessels from diabetic patients. J Med Imaging (Bellingham) 4, 014503. https://doi.org/10.1117/1.JMI.4.1.014503

30. Hoover, A.D., Kouznetsova, V., Goldbaum, M., 2000. Locating blood vessels in retinal images by piecewise threshold probing of a matched filter response. IEEE Transactions on Medical Imaging 19, 203–210. https://doi.org/10.1109/42.845178
31. Horwath, J.P., Zakharov, D.N., Mégret, R., Stach, E.A., 2020. Understanding important features of deep learning models for segmentation of high-resolution transmission electron microscopy images. npj Comput Mater 6, 1–9. https://doi.org/10.1038/s41524-020-00363-x
32. Huang, G., Liu, Z., van der Maaten, L., Weinberger, K.Q., 2018. Densely Connected Convolutional Networks. arXiv:1608.06993 [cs].
33. Huang, Z., Jiang, Z., Hu, Y., Hu, Y., Zou, D., Yu, Y., Ren, Q., Ren, Q., Ren, Q., Liu, G., Liu, G., Liu, G., Lu, Y., Lu, Y., Lu, Y., Lu, Y., 2020. Retinal choroidal vessel imaging based on multi-wavelength fundus imaging with the guidance of optical coherence tomography. Biomed. Opt. Express, BOE 11, 5212–5224. https://doi.org/10.1364/BOE.397750
34. Ikram, M.K., Witteman, J.C., Vingerling, J.R., Breteler, M.M., Hofman, A., De Jong, P.T., 2006. Retinal vessel diameters and risk of hypertension. The Rotterdam Study. American Journal of Ophthalmology 141, 601–602. https://doi.org/10.1016/j.ajo.2006.01.053
35. Kabedi, N.N., Kayembe, D.L., Mwanza, J.-C., Lepira, F.B., Kayembe, T.K., 2014. Hypertensive retinopathy and its association with cardiovascular, renal and cerebrovascular morbidity in Congolese patients. Cardiovasc J Afr 25, 228–232. https://doi.org/10.5830/CVJA-2014-045
36. Kamran, S.A., Hossain, K.F., Tavakkoli, A., Zuckerbrod, S.L., Sanders, K.M., Baker, S.A., 2021. RV-GAN: Segmenting Retinal Vascular Structure in Fundus Photographs using a Novel Multi-scale Generative Adversarial Network. arXiv:2101.00535 [cs, eess] 12908, 34–44. https://doi.org/10.1007/978-3-030-87237-3_4
37. Karlsson, R.A., Jonsson, B.A., Hardarson, S.H., Olafsdottir, O.B., Halldorsson, G.H., Stefansson, E., 2021. Automatic fundus image quality assessment on a continuous scale. Computers in Biology and Medicine 129, 104114. https://doi.org/10.1016/j.compbiomed.2020.104114
38. Kaur, C., Foulds, W.S., Ling, E.-A., 2008. Hypoxia-ischemia and retinal ganglion cell damage. Clin Ophthalmol 2, 879–889.
39. Khaledyan, D., Amirany, A., Jafari, K., Moaiyeri, M.H., Khuzani, A.Z., Mashhadi, N., 2020. Low-Cost Implementation of Bilinear and Bicubic Image Interpolation for Real-Time Image Super-Resolution, in: 2020 IEEE Global Humanitarian Technology Conference (GHTC). Presented at the 2020 IEEE Global Humanitarian Technology Conference (GHTC), IEEE, Seattle, WA, USA, pp. 1–5. https://doi.org/10.1109/GHTC46280.2020.9342625
40. Kushol, R., Salekin, M.S., 2020. Rbvs-Net: A Robust Convolutional Neural Network For Retinal Blood Vessel Segmentation, in: 2020 IEEE International Conference on Image Processing (ICIP). Presented at the 2020 IEEE International Conference on Image Processing (ICIP), pp. 398–402. https://doi.org/10.1109/ICIP40778.2020.9190759
41. Kusuhara, S., Fukushima, Y., Ogura, S., Inoue, N., Uemura, A., 2018. Pathophysiology of Diabetic Retinopathy: The Old and the New. Diabetes Metab J 42, 364–376. https://doi.org/10.4093/dmj.2018.0182
42. L Srinidhi, C., Aparna, P., Rajan, J., 2017. Recent Advancements in Retinal Vessel Segmentation. J Med Syst 41, 70. https://doi.org/10.1007/s10916-017-0719-2
43. Lambert-Cheatham, N., Jusufbegovic, D., Corson, T.W., 2021. Intraocular and Orbital Cancers, in: Reference Module in Biomedical Sciences. Elsevier. https://doi.org/10.1016/B978-0-12-820472-6.00024-4
44. Li, J., Hu, Q., Imran, A., Zhang, L., Yang, J., Wang, Q., 2018. Vessel Recognition of Retinal Fundus Images Based on Fully Convolutional Network, in: 2018 IEEE 42nd Annual Computer Software and Applications Conference (COMPSAC). Presented at the 2018 IEEE 42nd Annual Computer Software and Applications Conference (COMPSAC), pp. 413–418. https://doi.org/10.1109/COMPSAC.2018.10268

45. Li, T., Bo, W., Hu, C., Kang, H., Liu, H., Wang, K., Fu, H., 2021. Applications of Deep Learning in Fundus Images: A Review. arXiv:2101.09864 [cs, eess].
46. Liu, F., Ren, X., Zhang, Z., Sun, X., Zou, Y., 2021. Rethinking Skip Connection with Layer Normalization in Transformers and ResNets. arXiv:2105.07205 [cs].
47. Mahabadi, N., Al Khalili, Y., 2021. Neuroanatomy, Retina, in: StatPearls. StatPearls Publishing, Treasure Island (FL).
48. Memari, N., Ramli, A.R., Saripan, M.I.B., Mashohor, S., Moghbel, M., 2019. Retinal Blood Vessel Segmentation by Using Matched Filtering and Fuzzy C-means Clustering with Integrated Level Set Method for Diabetic Retinopathy Assessment. J. Med. Biol. Eng. 39, 713–731. https://doi.org/10.1007/s40846-018-0454-2
49. Miri, M., Amini, Z., Rabbani, H., Kafieh, R., 2017. A Comprehensive Study of Retinal Vessel Classification Methods in Fundus Images. J Med Signals Sens 7, 59–70.
50. Modi, P., Arsiwalla, T., 2022. Hypertensive Retinopathy, in: StatPearls. StatPearls Publishing, Treasure Island (FL).
51. Oliveira, A., Pereira, S., Silva, C.A., 2018. Retinal vessel segmentation based on Fully Convolutional Neural Networks. Expert Systems with Applications 112, 229–242. https://doi.org/10.1016/j.eswa.2018.06.034
52. Oluleye, S.T., Olusanya, B.A., Adeoye, A.M., 2016. Retinal vascular changes in hypertensive patients in Ibadan, Sub-Saharan Africa. Int J Gen Med 9, 285–290. https://doi.org/10.2147/IJGM.S107241
53. Owen, C.G., Rudnicka, A.R., Mullen, R., Barman, S.A., Monekosso, D., Whincup, P.H., Ng, J., Paterson, C., 2009. Measuring Retinal Vessel Tortuosity in 10-Year-Old Children: Validation of the Computer-Assisted Image Analysis of the Retina (CAIAR) Program. Invest. Ophthalmol. Vis. Sci. 50, 2004–2010. https://doi.org/10.1167/iovs.08-3018
54. Pappuru, R.K.R., Ribeiro, L., Lobo, C., Alves, D., Cunha-Vaz, J., 2019. Microaneurysm turnover is a predictor of diabetic retinopathy progression. Br J Ophthalmol 103, 222–226. https://doi.org/10.1136/bjophthalmol-2018-311887
55. Pauli, T.W., Gangaputra, S., Hubbard, L.D., Thayer, D.W., Chandler, C.S., Peng, Q., Narkar, A., Ferrier, N.J., Danis, R.P., 2012. Effect of Image Compression and Resolution on Retinal Vascular Caliber. Investigative Ophthalmology & Visual Science 53, 5117–5123. https://doi.org/10.1167/iovs.12-9643
56. Pednekar, G.V., Udupa, J.K., McLaughlin, D.J., Wu, X., Tong, Y., Simone, C.B., Camaratta, J., Torigian, D.A., 2018. Image Quality and Segmentation. Proc SPIE Int Soc Opt Eng 10576, 105762N. https://doi.org/10.1117/12.2293622
57. Piyasena, M.M.P.N., Yip, J.L.Y., MacLeod, D., Kim, M., Gudlavalleti, V.S.M., 2019. Diagnostic test accuracy of diabetic retinopathy screening by physician graders using a hand-held non-mydriatic retinal camera at a tertiary level medical clinic. BMC Ophthalmol 19, 89. https://doi.org/10.1186/s12886-019-1092-3
58. Rahman, S., Rahman, M.M., Abdullah-Al-Wadud, M., Al-Quaderi, G.D., Shoyaib, M., 2016. An adaptive gamma correction for image enhancement. EURASIP Journal on Image and Video Processing 2016, 35. https://doi.org/10.1186/s13640-016-0138-1
59. Ramos-Soto, O., Rodríguez-Esparza, E., Balderas-Mata, S.E., Oliva, D., Hassanien, A.E., Meleppat, R.K., Zawadzki, R.J., 2021. An efficient retinal blood vessel segmentation in eye fundus images by using optimized top-hat and homomorphic filtering. Computer Methods and Programs in Biomedicine 201, 105949. https://doi.org/10.1016/j.cmpb.2021.105949
60. Richter, M.L., Byttner, W., Krumnack, U., Schallner, L., Shenk, J., 2021. Size Matters. arXiv:2102.01582 [cs] 12892, 133–144. https://doi.org/10.1007/978-3-030-86340-1_11
61. Ronneberger, O., Fischer, P., Brox, T., 2015. U-Net: Convolutional Networks for Biomedical Image Segmentation, in: Navab, N., Hornegger, J., Wells, W.M., Frangi, A.F. (Eds.), Medical Image Computing and Computer-Assisted Intervention – MICCAI 2015, Lecture Notes in

Computer Science. Springer International Publishing, Cham, pp. 234–241. https://doi.org/10.1007/978-3-319-24574-4_28
62. Rosen, R.B., Romo, J.S.A., Krawitz, B.D., Mo, S., Fawzi, A.A., Linderman, R.E., Carroll, J., Pinhas, A., Chui, T.Y.P., 2019. Earliest Evidence of Preclinical Diabetic Retinopathy Revealed using Optical Coherence Tomography Angiography (OCTA) Perfused Capillary Density. Am J Ophthalmol 203, 103–115. https://doi.org/10.1016/j.ajo.2019.01.012
63. Rukundo, O., 2021. EFFECTS OF IMAGE SIZE ON DEEP LEARNING.
64. Rukundo, O., Cao, H., 2012. Nearest Neighbor Value Interpolation. International Journal of Advanced Computer Science and Applications (IJACSA) 3. https://doi.org/10.14569/IJACSA.2012.030405
65. Sahlsten, J., Jaskari, J., Kivinen, J., Turunen, L., Jaanio, E., Hietala, K., Kaski, K., 2019. Deep Learning Fundus Image Analysis for Diabetic Retinopathy and Macular Edema Grading. Sci Rep 9, 10750. https://doi.org/10.1038/s41598-019-47181-w
66. Sekou, T.B., Hidane, M., Olivier, J., Cardot, H., 2019. From Patch to Image Segmentation using Fully Convolutional Networks -- Application to Retinal Images. arXiv:1904.03892 [cs].
67. Semerád, L., Drahanský, M., 2020. Retinal Vascular Characteristics, in: Uhl, A., Busch, C., Marcel, S., Veldhuis, R. (Eds.), Handbook of Vascular Biometrics, Advances in Computer Vision and Pattern Recognition. Springer International Publishing, Cham, pp. 309–354. https://doi.org/10.1007/978-3-030-27731-4_11
68. Shen, Y., Sheng, B., Fang, R., Li, H., Dai, L., Stolte, S., Qin, J., Jia, W., Shen, D., 2020. Domain-invariant interpretable fundus image quality assessment. Medical Image Analysis 61, 101654. https://doi.org/10.1016/j.media.2020.101654
69. Soomro, T.A., Afifi, A.J., Gao, J., Hellwich, O., Paul, M., Zheng, L., 2018. Strided U-Net Model: Retinal Vessels Segmentation using Dice Loss, in: 2018 Digital Image Computing: Techniques and Applications (DICTA). Presented at the 2018 Digital Image Computing: Techniques and Applications (DICTA), pp. 1–8. https://doi.org/10.1109/DICTA.2018.8615770
70. Sosale, A.R., 2019. Screening for diabetic retinopathy—is the use of artificial intelligence and cost-effective fundus imaging the answer? Int J Diabetes Dev Ctries 39, 1–3. https://doi.org/10.1007/s13410-019-00729-y
71. Swathi, C., Anoop, B.K., Dhas, D.A.S., Sanker, S.P., 2017. Comparison of different image preprocessing methods used for retinal fundus images, in: 2017 Conference on Emerging Devices and Smart Systems (ICEDSS). Presented at the 2017 Conference on Emerging Devices and Smart Systems (ICEDSS), pp. 175–179. https://doi.org/10.1109/ICEDSS.2017.8073677
72. Triwijoyo, B., Adil, A., 2021. Analysis of Medical Image Resizing Using Bicubic Interpolation Algorithm. Jurnal Ilmu Komputer 14, 20–29. https://doi.org/10.24843/JIK.2021.v14.i01.p03
73. Tsukikawa, M., Stacey, A.W., 2020. A Review of Hypertensive Retinopathy and Chorioretinopathy. Clin Optom (Auckl) 12, 67–73. https://doi.org/10.2147/OPTO.S183492
74. V., S., G., I., 2021. Encoder Enhanced Atrous (EEA) Unet architecture for Retinal Blood vessel segmentation. Cognitive Systems Research 67, 84–95. https://doi.org/10.1016/j.cogsys.2021.01.003
75. Wan, C., Zhou, X., You, Q., Sun, J., Shen, J., Zhu, S., Jiang, Q., Yang, W., 2022. Retinal Image Enhancement Using Cycle-Constraint Adversarial Network. Frontiers in Medicine 8.
76. Wang, W., Lo, A.C.Y., 2018. Diabetic Retinopathy: Pathophysiology and Treatments. Int J Mol Sci 19, 1816. https://doi.org/10.3390/ijms19061816
77. Wong, T.Y., Sabanayagam, C., 2020. Strategies to Tackle the Global Burden of Diabetic Retinopathy: From Epidemiology to Artificial Intelligence. OPH 243, 9–20. https://doi.org/10.1159/000502387

78. Wong, T.Y., Wong, T., Mitchell, P., 2007. The eye in hypertension. Lancet 369, 425–435. https://doi.org/10.1016/S0140-6736(07)60198-6
79. Xiuqin, P., Zhang, Q., Zhang, H., Li, S., 2019. A Fundus Retinal Vessels Segmentation Scheme Based on the Improved Deep Learning U-Net Model. IEEE Access 7, 122634–122643. https://doi.org/10.1109/ACCESS.2019.2935138
80. Zapata, M.A., Royo-Fibla, D., Font, O., Vela, J.I., Marcantonio, I., Moya-Sánchez, E.U., Sánchez-Pérez, A., Garcia-Gasulla, D., Cortés, U., Ayguadé, E., Labarta, J., 2020. Artificial Intelligence to Identify Retinal Fundus Images, Quality Validation, Laterality Evaluation, Macular Degeneration, and Suspected Glaucoma . OPTH 14, 419–429. https://doi.org/10.2147/OPTH.S235751
81. Zhang, J., Dashtbozorg, B., Bekkers, E., Pluim, J.P.W., Duits, R., Romeny, B.M. ter H., 2016. Robust Retinal Vessel Segmentation via Locally Adaptive Derivative Frames in Orientation Scores. IEEE Transactions on Medical Imaging 35, 2631–2644. https://doi.org/10.1109/TMI.2016.2587062
82. Zhang, Z., Liu, Q., Wang, Y., 2018. Road Extraction by Deep Residual U-Net. IEEE Geosci. Remote Sensing Lett. 15, 749–753. https://doi.org/10.1109/LGRS.2018.2802944

SUMMARY

Master thesis “Investigation of eye fundus image quality on vascular segmentation using deep neural networks” was conducted at Vilnius university by the student of Systems biology master program Julija Domarkaitė. This master thesis investigates the impact of fundus image quality on deep neural networks performance on retinal vessel segmentation. Automatic segmentation of retinal vessels from fundus images provides information about vessels characteristics but models are unable to handle diverse data. This problem requires a deep investigation on the impact of image quality on deep neural network performance. In order to give insights, this master thesis analyses seven datasets of different properties and quality and their influence on the performance of two deep neural networks. The effects of image size, resizing technique and input size on the model performance are observed. This master thesis shows that models perform on diverse data differently and modifications of image size alter provided information to the models leading to changes in their performance. Different interpolation techniques create different pixel representations which affects segmentation results. Changes of input size provide different contextual information to the model which also affects the segmentation of retinal vessels. In conclusion, this master thesis evaluates the effects of quality of the images and various components on the segmentation of fundus images and provides valuable information about the best approaches to deal with diverse data.

SUMMARY IN LITHUANIAN

Vilniaus universiteto Sistemų biologijos magistrantūros studijų programos studentė Julija Domarkaitė atliko magistro baigiamąjį darbą „Akies dugno vaizdų kokybės poveikis kraujagyslių segmentavimui naudojant giliuosius neuroninius tinklus“. Šis magistrinis darbas tiria akies dugno nuotraukų kokybės įtaką giliųjų neuroninių tinklų veikimui segmentuojant tinklainės kraujagysles. Automatinis tinklainės kraujagyslių segmentavimas iš akies dugno vaizdų suteikia informacijos apie kraujagyslių savybes, tačiau automatiniai modeliai nesugeba tinkamai apdoroti duomenų pasižyminčių įvairiomis ir skirtingomis charakteristikomis. Ši problema reikalauja gilios analizės tyrinėjant vaizdų kokybės įtaką giliojo neuroninio tinklo veikimui. Tam, kad suteikti įžvalgų, šiame magistriniame darbe yra analizuojami septyni skirtingų savybių ir kokybės duomenų rinkiniai bei jų įtaka dviejų giliųjų neuroninių tinklų veikimui. Stebimi vaizdo dydžio, dydžio keitimo metodo ir įvesties dydžio poveikiai modelio veikimui. Šis magistro darbas parodo, kad modeliai skirtingai veikia įvairius duomenis, o vaizdo dydžio modifikacijos pakeičia modeliams paduodamą informaciją, taip darant įtaką jų veikimui. Skirtingi interpoliacijų metodai sukuria skirtingas pikselių pateiktis, kurie turi įtakos segmentavimo rezultatams. Įvesties dydžio pokyčiai suteikia modeliui skirtingą kontekstualią informaciją, kuri taip pat turi įtakos tinklainės kraujagyslių segmentavimui. Apibendrinant, šiame magistro darbe analizuojamas įvairių komponentų poveikis akių dugno vaizdų segmentavimui ir pateikiama vertingos informacijos apie geriausius būdus, kaip dirbti su įvairiais duomenimis.